

Multi-scale soil moisture data and process-based modeling reveal the importance of lateral groundwater flow in a subarctic catchment

Jari-Pekka Nousu^{1,2}, Kersti Leppä², Hannu Marttila¹, Pertti Ala-aho¹, Giulia Mazzotti³, Terhikki Manninen⁴, Mika Korhonen⁵, Mika Aurela⁵, Annalea Lohila^{5,6}, and Samuli Launiainen²

¹Water, Energy and Environmental Engineering Research Unit, P.O. Box 4300, 90014 University of Oulu, Finland

²Bioeconomy and Environment, Natural Resources Institute Finland, Helsinki, Finland

³Univ. Grenoble Alpes, Université de Toulouse, Météo-France, CNRS, CNRM, Centre d'Études de la Neige, Grenoble, France

⁴Meteorological Research, Finnish Meteorological Institute, P.O. Box 503, 00101, Helsinki, Finland

⁵Climate System Research, Finnish Meteorological Institute, P.O. Box 503, 00101, Helsinki, Finland

⁶Institute for Atmospheric and Earth System Research INAR, University of Helsinki, Helsinki, Finland

Correspondence: Jari-Pekka Nousu (jari-pekka.nousu@luke.fi)

Abstract. Soil moisture plays a key role in soil nutrient and carbon cycling, plant productivity and in energy, water, and greenhouse gas exchanges between the land and the atmosphere. [The knowledge on drivers of spatiotemporal soil moisture dynamics in subarctic landscape is limited.](#) In this study, we used the Spatial Forest Hydrology (SpaFH_y) model, *in-situ* soil moisture ~~measurements~~-[data](#) and Sentinel-1 SAR-based soil moisture estimates to explore spatiotemporal controls of soil moisture in a subarctic headwater catchment in northwestern Finland. The role of groundwater dynamics and lateral flow on soil moisture was studied through three groundwater model conceptualizations: i) omission of groundwater storage and lateral flow, ii) conceptual TOPMODEL approach based on topographic wetness index, and iii) explicit 2D lateral groundwater flow. The model simulations were compared against continuous ~~point-scale~~-[point soil moisture](#) measurements, distributed manual measurements~~conducted in the study area~~, and novel SAR-based soil moisture estimates available ~~from the area~~ at high spatial and temporal resolution. Based on model scenarios and model-data ~~comparisons~~[comparison](#), we assessed when and where the lateral groundwater flow shapes [shallow](#) soil moisture, and under which conditions soil moisture variability is driven more by local ~~ecohydrological processes~~[ecohydrology](#), i.e. the balance of infiltration, drainage and evapotranspiration. The choice of groundwater ~~conceptualization~~-[flow model](#) was shown to have a strong impact on ~~the~~-modeled soil moisture dynamics within the catchment. All model conceptualizations captured the observed soil moisture dynamics in the upland forests, but accounting for the lateral groundwater flow was necessary to reproduce the saturated conditions ~~commonly-occurring~~-[common](#) on the peatlands and occasionally on lowland forest grid-cells. We further highlight the potential of integrating multi-scale observations ~~, including spatially explicit remote sensing data,~~ with land surface and hydrological models. The results have ~~broad implications for choosing suitable models for studying~~-[implications for](#) ecohydrological and biogeochemical processes as well as ~~earth~~-[modeling hydrology and Earth](#) system feedbacks in subarctic and boreal environments.

20 1 Introduction

Soil moisture has a direct influence on land surface energy fluxes (Seneviratne et al., 2010; Ji et al., 2017), partitioning of precipitation into infiltration and runoff (Liu et al., 2019; Singh et al., 2021), and plant productivity and water use (Daly and Porporato, 2005; Lagergren and Lindroth, 2002). It is also a key variable controlling soil microbial activity and consequent greenhouse gas emissions (Bonan, 1990; Karhu et al., 2014; Lohila et al., 2016; Makhnykina et al., 2020), and soil carbon balance (Larson et al., 2023). In the boreal and subarctic region, ~~the~~ climate change is predicted to amplify seasonal variability of soil moisture due to longer and more frequent summer droughts, increased autumn and winter precipitation (Holmberg et al., 2014; Ruosteenoja et al., 2018), and changes in snow accumulation and melt (Räsänen, 2021). The altered soil moisture dynamics have an effect on the severity of abiotic stressors (e.g. water shortage, excess water, extreme temperatures) and biotic damages, ~~both~~ affecting tree health, mortality and forest productivity (Buermann et al., 2014; Muukkonen et al., 2015; Wang et al., 2023). The changes in soil moisture across the landscape can significantly impact vegetation dynamics and alter ~~the~~ competition between species, shaping the structures of the ecosystem (Venäläinen et al., 2020; Junttila et al., 2022; Ameray et al., 2023). Moreover, northern peatlands are sources of methane (Huttunen et al., 2003; Schneider et al., 2016) and boreal upland forests can turn from methane sinks to sources under long-lasting high soil moisture conditions (Korkiakoski et al., 2022; Lohila et al., 2016). Hence, accurate information on spatiotemporal soil moisture conditions has the potential to improve estimates of tree health, ~~carbon~~ terrestrial carbon stocks and greenhouse gas sinks and sources, ~~and nutrient leaching as well as lateral export of carbon and nutrients~~ (Bond-Lamberty et al., 2016; Nakhavali et al., 2021). Soil moisture dynamics is also critical for weather and hydrological forecasting (Zhang et al., 2020a; Joo and Tian, 2021), climate change impact studies (Seneviratne et al., 2010; Kløve et al., 2014; IPCC, 2019), and for developing sustainable forest management practices (Salmivaara et al., 2021; Kankare et al., 2019).

Soil moisture has strong spatiotemporal variability driven by hydrometeorological conditions, landscape heterogeneity, and hydrological connectivity through lateral groundwater flow (Corradini, 2014; Kemppinen et al., 2023; Kim and Mohanty, 2016; Ji et al., 2017). The unsaturated soil is bounded at the bottom by the water table, and exchanges between the saturated and unsaturated zone occur through upward capillary rise and downward percolation (Maxwell et al., 2007; Miguez-Macho et al., 2007; J.-P. Vergnes and Habets, 2014). The lateral groundwater flow and consequent ~~undulation of variation in~~ the water table depth influences soil moisture especially in areas with shallow water table such as riparian areas, floodplains, and peatlands (Krinner, 2003; Decharme et al., 2019; Kollet and Maxwell, 2008).

Information on soil moisture dynamics can be obtained via *in-situ* measurements and remote sensing, as well as using numerical models (Robinson et al., 2008; Yu et al., 2021; Dobriyal et al., 2012). Continuous automatic *in-situ* measurements are well suited to capture soil moisture patterns at high temporal resolution at point-scale (Moreno et al., 2022; Kemppinen et al., 2023). However, distributing the observation network in space requires significant resources (Tyystjärvi et al., 2022) and is thus restricted to specific study areas (Kemppinen et al., 2023). Recent advances in satellite remote sensing have shown the potential to obtain soil moisture estimates at high spatial resolution (e.g. Sentinel-1 Synthetic Aperture Radar (SAR): Quast et al. (2023); Bauer-Marschallinger et al. (2019); Manninen et al. (2021)), but their accuracy for high-latitude

forests is still limited (Celik et al., 2022). ~~Indeed, observational methods are proven to be useful to interpret the present~~
55 ~~and historical states but cannot inform future trends and conditions.~~ To predict soil moisture conditions under environmental
change, process-based hydrological models are a prerequisite. However, their development also relies largely on observa-
tions (Panday and Huyakorn, 2004; Tyystjärvi et al., 2022), and it is widely accepted that the integration of *in-situ* mea-
surements, remote sensing, and process-based modeling is the best avenue forward (~~Crow and Yilmaz, 2014; Sidle, 2021~~)
(Crow and Yilmaz, 2014; Sidle, 2021; De Lannoy et al., 2022). To yield accurate predictions, it is essential that process-based
60 models represent the most relevant local features and processes that affect soil moisture dynamics (Sidle, 2021; Ji et al., 2017;
Kollet and Maxwell, 2008).

Due to the proliferation of geospatial data on land use, topography, vegetation, and soil characteristics, spatially distributed
models can ~~to an increasing extent~~ incorporate spatial variability in their parameterizations, and ~~allow extending extend~~ point-
scale simulations to scales relevant for practical applications (Launiainen et al., 2019; Ma et al., 2016; Clark et al., 2015; Maneta
65 and Silverman, 2013). To model soil moisture at high spatial resolution, incorporating the effects of local soil texture and
vegetation, as well as the conceptualization of subsurface water storage and lateral flow become important. Integrated surface-
groundwater models can explicitly represent these interactions in 3D (Ala-aho et al., 2017a; Thornton et al., 2022; Autio et al.,
2023), but are rarely used in ecosystem studies or large-scale applications due to their vast data needs and low computational ef-
ficiency. ~~For instance, attention~~ Attention towards groundwater dynamics is rather recent in land surface models used in climate,
70 weather and hydrological modeling communities (~~Decharme et al., 2019; Kollet and Maxwell, 2008; Maxwell and Condon, 2016; Ji et al.,~~
(Decharme et al., 2019; Zeng et al., 2018; Li et al., 2022; Maxwell and Condon, 2016; Ji et al., 2017; Niu et al., 2014). In catch-
ment hydrological models, the lateral movement of groundwater is ~~still rarely explicitly addressed~~ also rarely explicitly described,
and the groundwater dynamics are often based on ~~simplified~~ conceptual approaches such as the use of topographic wetness
index (TWI) (Beven and Kirkby, 1979) or grid-cell independent groundwater buckets (Bergström, 1992). These simplified
75 approaches can efficiently link grid-cell and catchment water budgets and simulate sufficient discharge dynamics (Launiainen
et al., 2019). They can also accurately estimate soil moisture dynamics ~~in landscape at~~ locations, where water balance is mostly
driven by local processes, i.e. infiltration, vertical water percolation and evapotranspiration (ET), rather than lateral flow and
capillary rise (Tyystjärvi et al., 2022). However, once the impacts of lateral groundwater flow and a shallow water table be-
come more pronounced, models neglecting ~~lateral flow these processes~~ encounter obvious challenges to accurately simulate
80 soil moisture dynamics (Kollet and Maxwell, 2008). Consequently, they often exhibit dry biases that directly affect simulations
of soil evaporation and plant transpiration (Maxwell and Condon, 2016).

Hydrological models are currently advancing towards incorporating more processes at higher spatial resolution (Sidle,
2021; Wood et al., 2011), but model calibration and evaluation are still largely based on point-scale observations of soil
moisture, ET and stream discharge at catchment outlet (Ala-aho et al., 2017b; Launiainen et al., 2019), creating uncertain-
85 ties for spatiotemporal simulations (Koch et al., 2018). The persistent lack of spatial observations of hydrological fluxes and
water storages (model state variables) prevents leveraging the full potential of distributed models and available data on land-
scape characteristics. Recent advances in remote sensing to produce spatially explicit data of precipitation (~~Yu et al., 2022~~)
(Yu et al., 2022; Skofronick-Jackson et al., 2017) and ET (Bhattarai and Wagle, 2021), canopy and soil water content (Manni-

nen et al., 2021; Zhang and Zhou, 2015), snow ~~properties~~ cover (Meriö et al., 2023), and water table depth (Toca et al., 2023; 90 Räsänen et al., 2022; Isoaho et al., 2023) open new opportunities to evaluate (Niu et al., 2021) and in some cases calibrate (Koch et al., 2018) spatially distributed models. Such data are increasingly included in hydrological model-data assimilation (Li et al., 2023; Deschamps-Berger et al., 2022).

In this study, we assess the controls of ~~spatiotemporal soil moisture~~ soil moisture dynamics at the subarctic Pallas Lompolojängänoja headwater catchment in northern Finland. We combine analysis of multi-scale observations, including *in-situ* 95 continuous and manual soil moisture measurements (Marttila et al., 2021; Aurela et al., 2015), SAR-based spatiotemporal estimates (Manninen et al., 2021), and process-based hydrological modeling. We use the Spatial Forest Hydrology model (SpaFH; Launiainen et al., 2019) at high spatial resolution ($16 \times 16 \text{ m}^2$) with three alternative conceptualizations for groundwater storage and dynamics. ~~In particular, we focus~~ We focus particularly on the influence of a shallow water table and lateral groundwater flow, as well as vegetation heterogeneity on spatiotemporal soil moisture dynamics through the following research 100 questions:

1. Where ~~and when~~ does lateral groundwater flow affect the temporal variability of ~~top~~ shallow soil moisture?
2. How does the role of lateral groundwater flow compare to the impact of vegetation heterogeneity in shaping soil moisture patterns?
3. How do SAR-based soil moisture estimates compare with the models, and can they be useful in model evaluation?

105 To answer the research questions, we compare and contrast model predictions i) between model conceptualisations, ii) against point-scale ~~measurements of soil moisture~~ soil moisture data, and iii) against SAR-based soil moisture estimates available from the study area.

2 Materials and methods

2.1 Study site

110 Our study area is located in the Pallas area ($67^{\circ}59'N$ $24^{\circ}13'E$) in northwestern Finland (Fig. 1B,C). Pallas has over 85 years of meteorological observations (Lohila et al., 2015), and the area has been recently set up as an interdisciplinary platform for atmospheric, ecological, and hydrological research. It includes multiple eddy covariance (EC) stations measuring surface-atmosphere energy and greenhouse gas fluxes, and both manual and automated ecohydrological monitoring ~~at over a~~ range of ecosystem types (Marttila et al., 2021). The climate in the area is characterized as subarctic. The long-term annual (1991– 115 2020) mean temperature and mean annual precipitation at the Muonio weather station, located approximately 25 km west of Pallas, are -0.6°C and 532 mm, respectively (Jokinen et al., 2021). ~~A~~ The proportion of precipitation falling as snow is approximately 42 % (Marttila et al., 2021), and the seasonal snow cover persists from about October until May (Aurela et al., 2015). Particularly, we consider the Lompolojängänoja catchment (hereafter LJO, Fig. 1A), which has the total area of circa 4.5 km^2 with ~~altitudes~~ elevations varying between 268 m and 364 m a.s.l. Soils in the upland parts of the catchment are mainly

120 gravely sand and sandy tills, and vegetation cover varies from coniferous forests to various types of mires such as open fens, treed mires, and paludified forests. ~~The~~ Except for a few small roads and ditches, the area has had little human influence and can be considered mostly a pristine subarctic headwater catchment. Figure 1A gives an overview of the landscape and the main measurement locations in the LJO catchment.

EC flux data and the meteorological data used in this paper was collected from two ~~Finnish Meteorological Institute (FMI)~~ flux stations located in the catchment of Lompolojängänoja ~~-(Fig. 1A)~~. The forest site ~~;~~ Kenttäröva (ICOS Ecosystem associate site) ~~;~~ is a Norway spruce-dominated forest growing on podzol soil with the age of the trees varying from 90 to 250 years. The number of trees, 643 and 68 ~~live stems /~~ stems ha^{-1} for spruce and deciduous trees (mainly ~~Betula pubescens~~ Betula pubescens), has stayed the same since a survey in 2011 (Aurela et al., 2015). The dominant tree height is currently about 15.5 m and 11 m for spruce and ~~deciduous trees~~ Betula pubescens, respectively. In 2011, a mean one-sided leaf-area index (LAI) for Norway spruce and ~~birch~~ Betula pubescens was 2.0 and 0.1 $\text{m}^2 \text{m}^{-2}$, respectively (Aurela et al., 2015).

The mire site ~~;~~ Lompolojänkki (ICOS Ecosystem Class 2 site) is an open, mesotrophic sedge fen (Zhang et al., 2020b) with a maximum peat thickness of about 2.5 m (Mathijssen et al., 2014). The Lompolonjängänoja stream flows through the long and narrow fen, draining into a nearby lake Pallasjärvi. ~~According to a plant species and coverage measurement done at 200 points around the EC tower in 2018, the~~ The dominant vascular species ~~growing at the site and having a mean coverage higher than 0.5 % were Andromeda polifolia, Betula nana and B. pubescens, Carex spp., Equisetum spp., Eriophorum spp. are~~ Andromeda polifolia, Betula nana and B. pubescens, Carex spp., Equisetum spp., Eriophorum spp. The dominant moss species are ~~Sphagnum spp.~~ Sphagnum spp., whose coverage is about 50 %. ~~In 2018 sampling, the~~ The mean one-sided LAI ~~and the vegetation height were on average was~~ 1.4 $\text{m}^2 \text{m}^{-2}$ and 40 cm, respectively. the mean vegetation height 0.4 m in 2018.

2.2 Models

140 We used the Spatial Forest Hydrology model (SpaFHy; Launiainen et al., 2019), developed to predict spatial and temporal patterns of hydrological fluxes and state variables in the vegetation canopy, organic moss-humus layer, and ~~rootzone (top soil)~~. ~~Its original aim was to provide a simple and practically applicable framework to study the effects of landscape heterogeneity and management on catchment hydrology in boreal forests. SpaFHy was in top soil (rootzone).~~ SpaFHy has been tested for 9 EC-flux sites in Finland and Sweden (stand-scale; ET and soil moisture) and for 21 small boreal headwater catchments in Finland (catchment-scale; runoff dynamics and ET to precipitation ratio) in Launiainen et al. (2019). ~~Latently, it~~ It has been adapted to drained peatland forests (Leppä et al., 2020; Stenberg et al., 2022), extended with nutrient balance and leaching modules (Laurén et al., 2021), applied to model forest drought risks (Launiainen et al., 2022) and used to predict soil moisture dynamics in the arctic tundra (Tyystjärvi et al., 2022). Its aim is to provide a simple and practically applicable framework to study the effects of landscape heterogeneity, management and macroclimatic change on catchment hydrology in boreal and subarctic landscapes.

150 The original SpaFHy includes two groundwater conceptualizations: a free drainage approach (i.e. neglecting groundwater dynamics, SpaFHy-1D) and a TOPMODEL-based approach (i.e. groundwater return flow based on topographic wetness index, SpaFHy-TOP). In this study, we implemented a new submodel to represent the 2D lateral ~~groundwater~~ Darcy flow (SpaFHy-

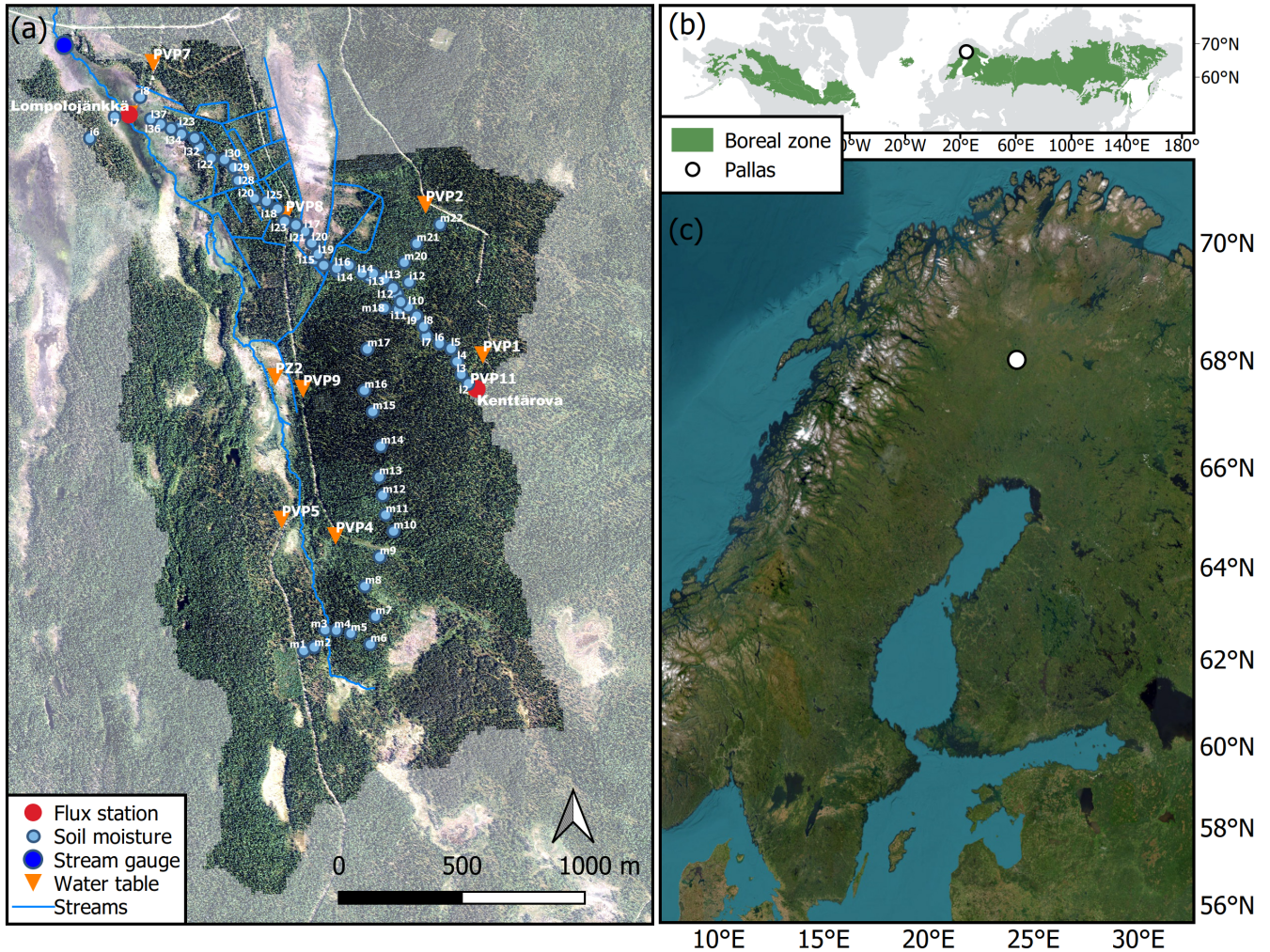


Figure 1. The Lompolojängänoja (LJO) catchment and its hydrological [measurements-measurement locations](#) (A, the aerial image by NLSF, 2020) is located in the northern boreal zone (B, green area, Olson et al., 2001) in northwestern Finland (C, Esri, 2023). The ICOS flux stations Kenttäröva ([forest](#)) and Lompolojängkä ([open mire](#)) are presented in red circles, stream gauge in blue, soil moisture measurement locations are labeled and presented in light blue, and water table depth monitoring locations are labeled and presented in orange. [Streams are shown as blue lines.](#)

2D). The salient features of the three model versions are briefly described next and summarized in Table 1. The general model parameters are given in Table 2.

2.2.1 SpaFHy-1D

SpaFHy-1D considers grid-cells as independent hydrological units (Launiainen et al., 2019). The hydrological processes in the vegetation canopy, snowpack, organic moss-humus layer, and rootzone are explicitly simulated at a daily timestep for each grid-cell in the model domain. The above-ground fluxes and state variables are computed in the canopy submodel, including rainfall and snowfall interception and evaporation, throughfall, transpiration, and snow accumulation and ~~melt-~~snowmelt (see Sect. 2.2. in Launiainen et al. (2019)). Snowmelt is computed with a degree-day approach while ET components are solved by the Penman–Monteith equation. For transpiration, the canopy conductance is derived from the stomatal optimality principle and accounting for an exponential attenuation of light in the canopy (Launiainen et al., 2019). The bucket submodel describes top soil hydrology and soil moisture dynamics in two layers. The upper layer is the organic moss-humus layer, whose water budget is affected by ~~intereception-and~~throughfall and snowmelt interception and soil evaporation, as well as infiltration to the lower rootzone layer, where drainage and transpiration take place. The lateral water flow between the grid-cells is omitted, and drainage from the bucket submodel is removed from the model domain as stream discharge at the catchment outlet without a delay. Thus, SpaFHy-1D represents a situation where soil moisture variability within the catchment is driven ~~only-solely~~ by the heterogeneity of vegetation, soil characteristics, and meteorological forcing. Similar conceptualizations of soil hydrology are common for large-scale land surface ~~models (Smith et al., 2001; Noilhan and Mahfouf, 1996)-and hydrological models (Smith et al., 2001; Seibert and Vis, 2012; Clark et al., 2008; Niu et al., 2011).~~The canopy and bucket submodels are common to all three SpaFHy versions.

2.2.2 SpaFHy-TOP

SpaFHy-TOP includes a conceptual description of the saturated zone using the TOPMODEL approach (Beven and Kirkby, 1979). Drainage from the bucket submodel feeds TOPMODEL's lumped catchment groundwater storage, which is then spatially distributed via the topographic wetness index (TWI). The TWI is defined as the natural logarithm of the flow accumulation area (i.e. upslope area draining through the grid-cell) divided by the tangent of the local slope ~~-Moreover, the (Beven and Kirkby, 1979). The~~ local saturation deficit is related to the TWI and catchment average saturation deficit, creating a higher probability for grid-cells with greater TWI to become saturated. During a model timestep, return flow from ~~the~~ groundwater storage to ~~the~~ rootzone and organic moss-humus layer occurs in grid-cells where ~~the~~ local saturation deficit is zero (Launiainen et al., 2019). The return flow is routed through ~~the~~ rootzone and the organic moss-humus layer and their respective soil moisture ~~is~~ updated, while ~~the~~ potential excess water becomes surface runoff. ~~Catchment discharge~~Discharge at the catchment outlet is the sum of ~~the~~ catchment average baseflow (predicted by TOPMODEL) and surface runoff without a delay. This version of SpaFHy-TOP is identical to the one used in Launiainen et al. (2019, 2022).

185 2.2.3 SpaFHy-2D

SpaFHy-2D version was developed in this study to ~~include an explicit description of the~~ explicitly describe lateral groundwater flow within the catchment. The modeling domain consists of soil columns whose relative elevation to one another is defined by the digital elevation model. Each soil column extends to an impermeable layer (no-flow boundary) at a predefined depth, while the columns are characterized by their water retention characteristics (following the van Genuchten -model; van Genuchten, 1980) and saturated hydraulic conductivity based on the soil type.

Lateral flow in the saturated zone is solved using the 2D groundwater flow equation:

$$C \frac{\partial h}{\partial t} = \frac{\partial h}{\partial x} \left(T \frac{\partial h}{\partial x} \right) + \frac{\partial h}{\partial y} \left(T \frac{\partial h}{\partial y} \right) + S \quad (1)$$

where t is time (d), x and y are the horizontal dimensions (m), C is the storage coefficient (m m^{-1}), T is transmissivity ($\text{m}^2 \text{d}^{-1}$), h is the hydraulic head (m), and S (m d^{-1}) is water drained from the overlaying bucket submodel. Lateral ~~flow~~ groundwater flow between grid-cells takes place only in the saturated zone, and thus T is obtained by integrating the saturated hydraulic conductivity over the saturated layer depth. C describes the change in h relative to a change in the soil column water content W (m). The relation between h and W is solved based on the assumption that in the unsaturated zone the water content profile sets to hydraulic equilibrium (constant hydraulic head in vertical dimension; Skaggs, 1980). For numerical efficiency of solving Eq. 1, interpolation functions for $W(h)$, $T(h)$, and $C(h)$ were constructed prior to simulation for each soil column type (Laurén et al., 2021). When the soil column becomes oversaturated, i.e. groundwater level rises to rootzone, the excess water is routed as return flow to the bucket submodel, similarly as in SpaFHy-TOP.

Streams (and ditches) in the catchment were described as ~~cells-grid-cells~~ with constant h , ~~and the~~ The outflow to streams is computed ~~based on from~~ the local hydraulic head gradient when the surrounding water table level is above the stream h . No flow from stream to soil is allowed. We do not consider temporal changes in stream water level and omit channel flow in the stream network; thus the sum of the outflow into the stream cells and surface runoff form the runoff ~~from the catchment at the catchment outlet without a delay. The assumption of a constant stream water level simplifies the modeling framework and should not significantly impact catchment soil moisture dynamics.~~ Catchment borders are defined as no flow boundaries, assuming no significant water flows occur between the delineated catchment and its surroundings that impact shallow soil moisture.

210 2.3 Model input

2.3.1 Geospatial data

To set up SpaFHy for the LJO catchment, we used mainly open geospatial data that is available throughout Finland. The rasters used are presented in Fig. 2, and summarized in Table 1.

For canopy attributes and for distinguishing between forest soils and mires, we used the multi-source National Forest Inventory (mNFI; Mäkisara et al., 2016) data at 16 m horizontal resolution. This was also chosen as the model grid resolution for the simulations, and other input rasters were aggregated accordingly, consistent with Launiainen et al. (2019). From mNFI data,

Table 1. Geospatial data used by each submodel, and submodel used by each model configuration.

Geospatial data	Canopy	Bucket	TOPMODEL	2D Flow
Digital elevation model			✓	✓
Catchment mask	✓	✓	✓	✓
Topographic wetness index			✓	
Shading coefficient	✓	✓		
Site class		✓		
Leaf area index	✓			
Canopy height	✓			
Canopy fraction	✓			
Soil type		✓		✓
Streams				✓

Model configuration	Canopy	Bucket	TOPMODEL	2D Flow
1D	✓	✓		
TOP	✓	✓	✓	
2D	✓	✓		✓

Geospatial data used by each submodel, and submodel

used by each model configuration.

needle and leaf mass rasters were used to derive one-sided LAI of deciduous and coniferous trees. LAI values were estimated using specific one-sided leaf areas for pine, spruce and birch (6.8, 4.7 and 12.0 m² kg⁻¹, respectively; Härkönen et al., 2015). LAI estimates of shrub and grass were adopted from local multi-source remote sensing data by Räsänen et al. (2021). The canopy fraction and prevailing site class (used for parameterizing the organic moss-humus layer) were also obtained from the mNFI data.

The soil type affects the hydraulic properties of the rootzone and the SpaFHy-2D lateral groundwater flow module. A combined soil type raster was constructed by taking the peatland boundaries from the National Land Survey of Finland topographic map NLSF (2020) and the remaining soil characteristics from the Geological Survey of Finland soil texture map (GSF, 2020) similarly to Launiainen et al. (2019).

The catchment was delineated based on the digital elevation model (NLSF, 2020) with Whitebox GAT software (Lindsay, 2014). TWI was calculated using the slope and flow accumulation raster, with the flow accumulation determined through the D8 method (O'Callaghan and Mark, 1984). The stream network was obtained from NLSF (2020). Furthermore, topographic impacts for solar radiation were considered by computing a daily shading coefficient, calculated as the potential daily radiation input for each grid-cell normalized by the potential input at the grid-cell of the Kenttäröva station, where the global radiation forcing was measured (see Sect. 2.3.2).

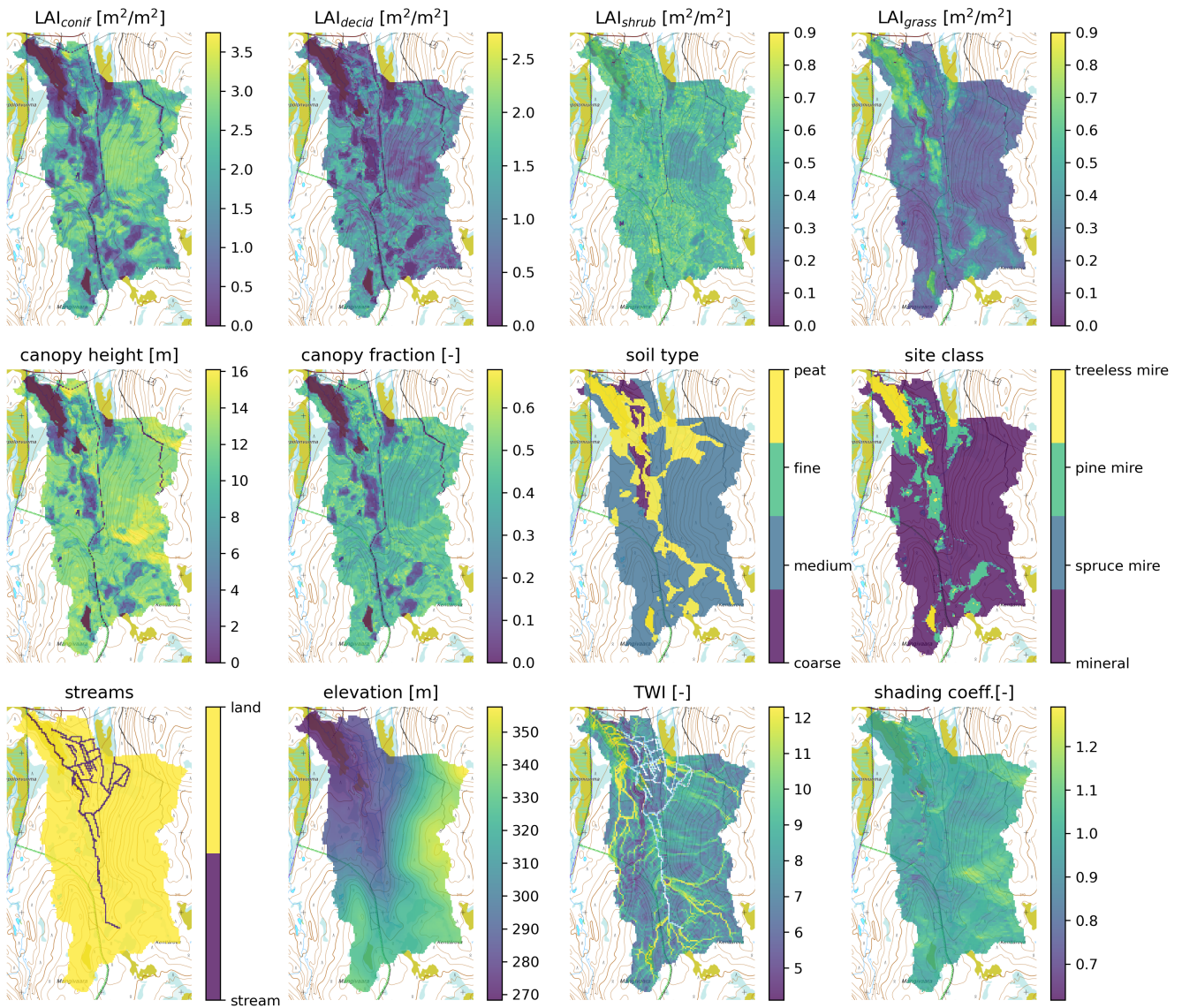


Figure 2. Set of geospatial rasters used to set up the model for the LJO catchment. Top row shows leaf-area index (LAI) for different plant types. For each grid-cell, the conifer and deciduous LAI forms the canopy LAI, and understory LAI is the sum of shrubs and grasses. TWI is the topographic wetness index. The rasters overlay a topographic map (NLSF, 2020).

2.3.2 Meteorological forcing

All SpaFHy versions require the same daily meteorological forcing: mean air temperature T_a ($^{\circ}\text{C}$), global radiation R_g (Wm^{-2}), relative humidity RH (%), wind speed U (m^{-1}) and daily accumulated precipitation P (mm). This data was compiled
235 and made available by Nousu et al. (2023), and includes *in-situ in-situ* observations at Kenttäröva station available from the Finnish Meteorological Institute (FMI) open database (FMI, 2021), supplemented by FMI's R_g observations from the Kenttäröva station (located at the hilltop, Fig. 1). The data gaps in R_g were first filled by data from contiguous sites and then by ERA5 reanalysis data (Hersbach et al., 2020). We multiplied the R_g forcing by the shading coefficient (see Sect. 2.3.1) for each day (Fig. 2) to account for the topographic effects on the radiation forcing at each grid cell. For the other meteorological
240 variables, a spatially uniform forcing was applied.

2.4 Model parameterization

The canopy and bucket submodels were common to all model versions and parameterized as in Launiainen et al. (2019). The only exception was the organic moss-humus layer, which was refined to allow for full or partial saturation in situations where upward return flow occurs from the rootzone layer. Drainage from the organic moss-humus layer to the rootzone layer
245 is represented identically as the drainage from the rootzone layer (Eq. 18 in Launiainen et al. (2019)). A depth of 0.05 m was assigned to the organic moss-humus layer (Table 2). To account for the different hydraulic properties of the organic moss-humus layer in mineral forest soils (dominated by feather mosses) and peatlands (mainly Sphagnum moss), the moss hydraulic parameters (porosity, field capacity, and relative available water ~~parameter~~) were derived from Williams and Flanagan (1996) and Elumeeva et al. (2011). The peatlands and mineral soils were separated based on mNFI site class (see Fig. 2); the site class
250 and soil type -specific parameters for the organic moss-humus, rootzone and deep ~~layers are presented~~ soil layers are given in the Supplement (Table S1–S3). Available literature was used to define the van Genuchten (1980) water retention parameters for the Bucket and 2D Flow submodels (Autio et al., 2023; Menberu et al., 2021). The rootzone was assigned a depth of 0.30 m (Table 2). Due to a lack of reliable data on the depth-to-bedrock, a uniform thickness of 5 m was assigned for the deep soil layer of the 2D groundwater module throughout the model domain. This estimate corresponds approximately to the
255 thickest peat layers and the shallowest mineral soil depths of the catchment (Autio et al., 2023). Canopy parameters for surface conductance for evaporation from the wet forest floor (G_f) and canopy storage capacity for rain (w_{max}), and the TOPMODEL effective soil depth parameter were obtained from Launiainen et al. (2019). No further calibration or sensitivity tests of any model parameters was/were conducted in this study.

Model simulations with the three different treatments of groundwater dynamics (named 1D, TOP and 2D) were run with
260 identical meteorological forcing, geospatial inputs (Fig. 2), and canopy and bucket submodel parameterizations (Table 2). To study how spatially heterogeneous vegetation affects soil moisture, additional 1D simulation was run with site class specific mean vegetation parameters. This experiment is referred to as $1D_{homog.canopy}$, and vegetation characteristics at each grid-cell belonging to a certain site class (Fig. 2) were set to the average of that particular site class (see Fig. S2S1). All simulations

cover period from 2011-01-01 to 2021-09-01, of which the beginning until 2013-09-01 was considered as a model spin-up
265 period and omitted from subsequent analysis.

2.5 Hydrological observations

This study benefits from the extensive hydrological monitoring of the LJO catchment (Marttila et al., 2021; Aurela et al., 2015). We further conducted several campaigns to measure spatiotemporal variability of soil moisture (i.e. volumetric water content θ) during 2019–2021. In particular, during snow-free seasons, biweekly manual measurements at 15 different points
270 (denoted as "i" in Fig. 1) were conducted using WET-2 and PR2 Profile Probe sensors with an HH2 readout unit (Delta-T Devices Ltd., Cambridge, U.K.) sampling soil moisture profile at depths 0 cm, 10 cm, 20 cm and 30 cm (from the soil surface). Additionally, we conducted two extended soil moisture measurement campaigns, including 56 additional locations -(denoted as "l" and "m" in Fig. 1). The first (2021-06-17) represents wet condition when soil moisture was still highly impacted by the snow-meltsnowmelt. The second (2021-09-01) was conducted in early autumn conditions after a precipitation event. Both
275 these campaigns used the sensor ML3 ThetaProbe (Delta-T Devices Ltd., Cambridge U.K.) that measures soil moisture at 5 cm depth. For the ML3 ThetaProbe sensor, soil moisture at locations with peat soils at full saturation were assigned directly to the assumed peat porosity (0.880.89).

In addition, we used data from continuous soil moisture sensors distributed in close proximity to the Kenttäröva flux site; covering the period from 2013 to 2021. From 2013 to 2017, soil moisture was continuously measured by four ThetaProbe
280 type ML2x sensors at 5 cm and 20 cm depths (two each) (Aurela et al., 2015). In 2017, more sensors were installed alongside the existing ones, among which we used two sensors (Soil Scout Oy, Helsinki, Finland) at depths 5 cm and 30 cm (from the soil surface). The continuous soil moisture measurements were averaged into daily values. To overcome the inherent uncertainties in *in-situ* measurements of soil moisture, stemming from different devices and measurement and installation procedures (Robinson et al., 2008; Dobriyal et al., 2012; Iwata et al., 2017), we present the means and variability ranges of
285 continuous soil moisture sensors, and address these uncertainties by averaging multiple manual probings within the area of interest within approximately a 5 m radius. All soil moisture measurements from 0 to 30 cm depth correspond to the rootzone layer of SpaFHy. As soil moisture of the organic moss-humus layer was not directly measured, we assume soil moisture measurements at the soil surface (0 cm depth) to best represent this layer.

ET was measured by the eddy covariance (EC) technique at the two flux stations, Kenttäröva spruce forest and Lompolo-
290 jänkkä peatland (Fig. 1A). The EC systems consist of USA-1 (METEK) 3D sonic anemometer and closed-path LI-7000 (Li-cor, Inc.) CO₂/H₂O analysers (Aurela et al., 2015). The procedure for obtaining the ET fluxes from eddy covariance data is given EC data processing is described in detail in Aurela et al. (2015) and in Nousu et al. (2023).

The runoff was measured by the Finnish Environment Institute with a 120-degree V-notch weir at the outlet (see stream gauge in Fig. 1A). Snow data consisted of automated snow depth observations at the Kenttäröva flux station, and approximately
295 monthly manual snow water equivalent (SWE) measurements at Kenttäröva and Lompolojänkkä flux-stations (Marttila et al., 2021).

2.6 SAR-based soil moisture estimates

We used SAR-based surface soil moisture estimates from the study area. This newly derived research data set was developed by Manninen et al. (2021), who used Sentinel-1 Synthetic Aperture Radar (SAR) ground range detected high-resolution data to produce high-resolution spatiotemporal soil moisture estimates of midday. The soil moisture estimates are retrieval using SAR images is based on the gradient boosted trees machine learning method trained with and boosting method, utilizing input variables of nonlocally averaged VH and VV backscattering coefficients, multitemporal SAR statistics, terrain data, effective LAI estimates based on SAR, SAR overpass information, and the time for the soil moisture estimate to be calculated. Distinct algorithms were developed for morning and evening flyovers, both relating soil moisture estimates to instantaneous midday. They were validated against discrete and continuous in-situ in-situ soil moisture measurements at Pallas (Manninen et al., 2021). In particular, the gradient boosted trees method was methods were trained with manual surface soil moisture measurements (depth = 0 cm) and continuous soil moisture measurements at deeper soil layers that were converted to surface conditions via linear regression in order to correspond to the penetration depth of the C-band SAR signal in soil, which is in the range of 1–5 cm (Beale et al., 2021; Nolan and Fatland, 2003). Distinct algorithms were developed for morning and evening flyovers, both relating estimates to instantaneous midday. Manninen et al. (2021) reported RMSEs of $0.065 \text{ m}^3\text{m}^{-3}$ and $0.088 \text{ m}^3\text{m}^{-3}$, and maximum errors of $0.341 \text{ m}^3\text{m}^{-3}$ and $0.339 \text{ m}^3\text{m}^{-3}$ for morning and evening satellite flyover estimates, respectively. Yet, the validity of the method could be checked only at 92 different locations, for which soil moisture data was available: altogether 678 discrete values not matching the overpass times of the SAR satellite and eight points of continuous data. Hence, Manninen et al. (2021) state that the spatially very limited in-situ dataset did not allow to conclude that the derived soil moisture maps would have the same soil moisture accuracy in the pixel resolution as the individual pixels used for developing and validating the soil moisture retrieval method. The reason for the morning images to have slightly smaller RMSE values than evening images was that several discrete soil moisture measurement points were in the distal slopes of the evening SAR images and prone to shading.

Further details on the SAR data can be found in Manninen et al. (2021). In this study, the original irregular grid-grids with approximately 10 m pixel spacing was were averaged into a 16 m regular grid using subpixel area weights to be compared with the model outputs.

2.7 Evaluation methods

Annual periods are defined as hydrological years starting from September (e.g., 2016 = 2015-09-01 to 2016-08-31). We use performance metrics of mean absolute error (MAE), mean bias error (MBE) and coefficient of determination (R^2) for model-data comparison. Moreover, we use the Kling-Gupta Efficiency (KGE) (Gupta et al., 2009) for comparing daily runoffs between simulations and observations. Mean differences (MD) are computed to compare different simulations (i.e. the mean difference at each grid-cell).

Table 2. [Parameters used by each submodel. Soil type- and site type-specific parameters are listed in the Supplement \(Tables S1-S3\).](#)

Parameter	Value	Units	Explanation	Note
Canopy				
A_{max}	10	$\mu\text{mol m}^{-2} \text{s}^{-1}$	maximum leaf net assimilation rate	Launiainen et al. (2019)
$g_{1,c}$	2.1	$\text{kPa}^{0.5}$	stomatal parameter for conifers	Launiainen et al. (2015)
$g_{1,d}$	3.5	$\text{kPa}^{0.5}$	stomatal parameter for deciduous	Lin et al. (2015)
b	50	Wm^{-2}	half-saturation PAR of light response	Launiainen et al. (2019)
k_p	0.6	-	radiation attenuation coefficient	Launiainen et al. (2019)
r_w	0.2	-	critical relative extractable water	Lagergren and Lindroth (2002)
$r_{w,min}$	0.02	-	minimum relative conductance	Launiainen et al. (2019)
G_f	0.01	ms^{-1}	surface conductance for evaporation from wet forest floor	Launiainen et al. (2019)
w_{max}	1.5	mm LAI^{-1}	canopy storage capacity for rain	Launiainen et al. (2019)
$w_{max,snow}$	4.5	mm LAI^{-1}	canopy storage capacity for snow	Pomeroy et al. (1998), Essery et al. (2003)
K_m	2.5	mm d^{-1}	melt coefficient in open area	Kuusisto (1984)
K_f	0.5	mm d^{-1}	freezing coefficient	Koivusalo and Kokkonen (2002)
Y_{max}	18.5	$^{\circ}\text{C}$	phenology model parameter	Kolari et al. (2007)
τ	13	d	time constant	Kolari et al. (2007)
$T_{0,y}$	-4	$^{\circ}\text{C}$	base temperature	Kolari et al. (2007)
Bucket				
$z_{s,org}$	0.05	m	organic layer depth	Launiainen et al. (2019)
$z_{s,root}$	0.3	m	root zone depth	Kalliokoski et al. (2010)
TOPMODEL				
T_0	0.001	m s^{-1}	transmissivity at saturation	Launiainen et al. (2019)
m	0.05	m	effective soil depth	Launiainen et al. (2019)
2D Flow				
$z_{s,deep}$	5	m	deep soil layer thickness	assigned
z_{stream}	-0.2	m	stream water level relative to surface elevation	assigned

Parameters used by each submodel

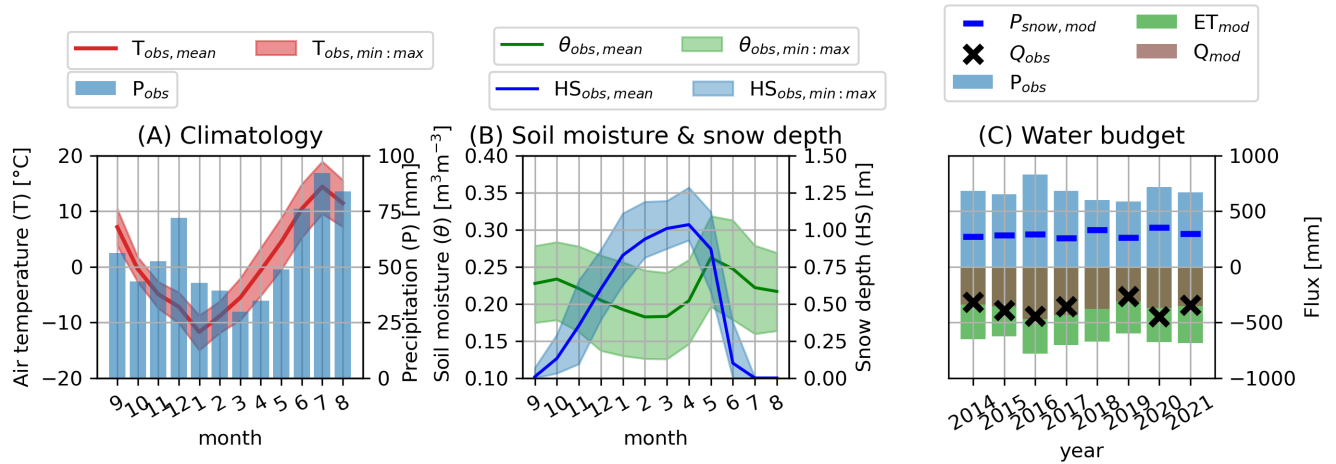


Figure 3. Hydrometeorological characteristics of Pallas. (A) Monthly observed climatology for the simulation period, (B) monthly observed volumetric soil moisture (θ) and snow depth (HS) at Kenttäröva forest site. The air temperature (T) and θ envelopes represent minimum and maximum monthly averages during simulation period, while the snow depth envelope shows minimum and maximum of monthly maximum during simulation period. (C) Annual water budget as observed (obs) and simulated (mod) with SpaFHy-2D, where Q is catchment runoff, ET evapotranspiration, P_{obs} is observed precipitation, and $SWE-P_{snow,mod}$ is modeled snow water equivalent precipitation. The change in catchment water storage (including canopy water, soil water and groundwater storage) $dS/dt = P + ET + Q$ is not shown. (B) ~~Monthly observed climatology and (C) monthly observed volumetric soil moisture and snow depth at Kenttäröva forest site. The air temperature and soil moisture envelopes represent minimum and maximum monthly averages of different years, while the snow depth envelope shows minimum and maximum of monthly maximums of different years.~~ Due to gaps in runoff measurements in 2018, runoff observation Q_{obs} is not ~~presented~~ available for 2018.

3 Results

3.1 Climatology and water budget dynamics

330 ~~Figure 3 introduces the main hydrometeorological characteristics of the LJO catchment.~~

As typical for high-latitudes, the period with permanent snow cover and freezing temperatures is long (Fig. 3B, ~~C~~, A, B), with nearly half of the annual precipitation falling as snow (250 mm – 350 mm, Fig. 3A, C), resulting in annual peak snow depths from approximately 0.9 to 1.3 m. ~~The snow melt (Fig. 3B). The snowmelt~~ period commonly spans roughly from late April to the beginning of June, resulting in the highest soil moisture ~~values during snowmelt~~ (Fig. 3C, B). The summer is characterized
 335 by cool to warm temperatures and higher precipitation that typically peaks in July (Fig. 3B, A).

Due to energy limitations for annual ET and large peak SWE, runoff dominates the water balance covering 49 to 67% of annual precipitation, while ET represents 34 to 50% depending on the year (Fig. 3C). SpaFHy-2D is able to closely capture the observed annual runoff during the simulated years (Fig. 3A, C). Also ~~the~~ daily runoff dynamics are reasonably well represented by both SpaFHy-TOP (KGE: 0.63) and SpaFHy-2D (KGE: 0.65) ~~(, see Fig. S1S2)~~. The summer runoff dynamics ~~followed~~

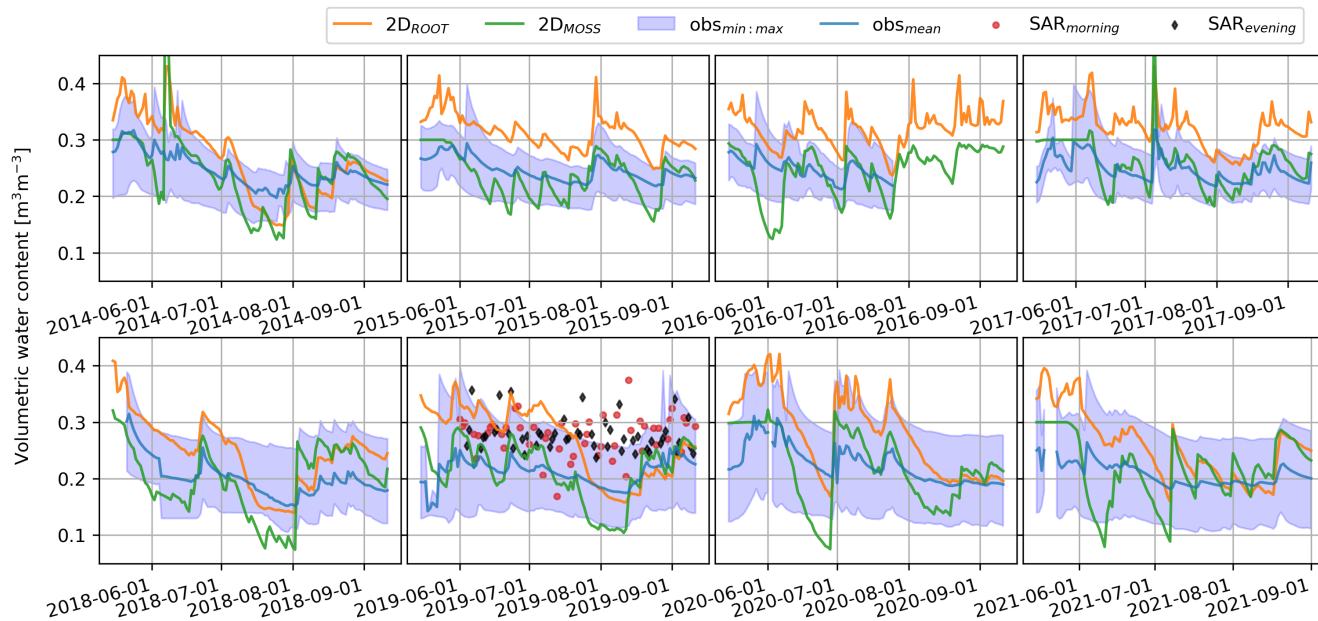


Figure 4. Temporal dynamics of soil moisture at Kenttäröva spruce forest simulated by SpaFHy-2D (rootzone and organic moss-humus layers), measured *in-situ in-situ* and estimated from SAR for 2014–2021 during May–Sept period. [Simulations and SAR-based estimates correspond to the mean of the nearby grid cells \(\$64 \times 64 \text{ m}^2\$ grid northwest of Kenttäröva\).](#) [The SAR-based surface soil moisture estimates are only available in 2019.](#)

340 [by-after](#) precipitation events are better captured by the 2D approach, whereas the baseflow is better predicted by TOP (Fig. [S1S2](#)). The simulations of [snow-water-equivalent-SWE](#) also align relatively well with the observations at Kenttäröva and Lompolojännkä (Fig. [S4S3](#)). Although catchment-scale ET observations are not available, the good performance in reproducing Q/P-ratio (Fig. [3AC](#)) means annual ET is also well described. This is in accordance with the relatively good correspondence between simulated and EC-measured daily ET from Lompolojännkä mire and Kenttäröva spruce forest [flux sites](#) (Fig. [S5S4](#)).

345 SpaFHy has also shown earlier to well reproduce the EC-based ET across the range of boreal and subarctic forests and peatlands (Launiainen et al., 2019).

3.2 Comparison of temporal soil moisture [dynamics at different locations with in-situ observations](#)

[Figure 4](#) shows the intra-seasonal dynamics of observed and simulated (SpaFHy-2D) soil moisture at the Kenttäröva site (Fig. 1A) for 2014–2021. In particular, the continuous measurements around Kenttäröva are compared to the simulated and SAR-estimated mean of the nearby grid cells ($64 \times 64 \text{ m}^2$ grid northwest of Kenttäröva). The 1D and TOP predictions were nearly identical to 2D at this hilltop area that contributes to groundwater recharge but where top soil moisture is not influenced by water table dynamics. The SAR-based surface soil moisture estimates are only available in 2019. Snow melt results in high soil moisture content in late May and beginning of June. The complete-

350

Intra-seasonal continuous *in-situ* data allow analysis of temporal soil moisture dynamics, and evaluation of models and SAR data (Fig. 4). Soil moisture peaks during snowmelt, and the date of complete snow melt-out of the snowpack can be detected as the corresponds to date when the modeled organic moss-humus layer moisture content begins to decrease due to evaporation: drop due to evaporative drying (Fig. 4). Later in the summer, the soil moisture dynamics are driven by intermittent precipitation events and more continuous drying by ET and drainage, with the general drying trend being dominant (Figs. 4 and 5).

At Kenttäröva hilltop area (Fig. 1A), which contributes to groundwater recharge, the SpaFHy-1D and TOP predictions were nearly identical to SpaFHy-2D. The modeled organic moss-humus layer acts as an interception storage, and its moisture content responds quickly to precipitation and evaporation. The model overestimates the mean well captures the seasonal trend but tends to overestimate both rootzone soil moisture content and its temporal change compared to point-scale observations in the rootzone at Kenttäröva: variability compared to the mean of point observations (Fig. 4, MBE: $0.05 \text{ m}^3 \text{ m}^{-3}$). This mismatch could potentially be corrected by calibrating soil field capacity and wilting point. However, as the comparison only represents one grid-cell, such calibration was not considered meaningful for the aims of this study. The SAR-based soil moisture estimates mostly fall in the observed range, especially those from the morning flyovers. The SAR morning flyover is in line with the main simulated and observed temporal dynamics, drying in June and wetting in late August. However, there is noticeable noise, and the temporal patterns of SAR morning and evening flyovers are different. A shift between the two flyovers can be noted; the wetter estimates come from the evening flyover, while the morning flyover predicts generally drier soil conditions.

Soil moisture dynamics in 2019, with SAR estimates available, were further assessed at eight additional biweekly measurement locations (Fig. 5). These include two forest, three peatland and three mixed forested-peatland grid-cells. The SAR-based estimates fall simulations mostly fall within the observed range corresponding to measurements at different soil depths. A systematic shift between SAR morning and evening flyover is again noticeable (up to 0.2 (MBE: $-0.01 \text{ m}^3 \text{ m}^{-3}$)). The temporal variability and seasonal patterns of the SAR estimates, especially of the evening flyovers, are small and do not follow the simulated or *in-situ* observed moisture dynamics. The morning flyover occasionally captures some temporal dynamics observed and simulated (see e.g. Fig. 5D). The SAR-based estimates do not reach the highest observed or simulated values, likely because they integrate information from multiple signals within a given grid-cell that have been averaged to correspond to the model grid when compared to observed maximum) and the comparison in Fig. 4 represents a single location, such calibration was not considered meaningful for the aims of this study.

The SpaFHy-2D also reasonably well predicts the rootzone soil moisture differences between the locations reasonably well locations, especially in terms of ranking the locations between wet, intermediate and dry (Fig. 5). The SAR-based soil moisture lacks the observed temporal variation whereas Minor discrepancies between SpaFHy-2D simulations tend to overestimate temporal dynamics compared to the *in-situ* observations: predicted rootzone and *in-situ* measured shallow soil moisture content are likely due to uncertainties in soil hydraulic parameters (e.g. too large field capacity in Fig. 5A). The moisture content of the organic moss-humus layer above the rootzone has stronger seasonal variability, and deviates from that of soil moisture is more dynamic than rootzone moisture, as evaporative losses exceed throughfall input leading to drying of the organic moss-humus layer from mid-July to end of August (Fig. 5). SpaFHy-2D does not include capillary rise from the rootzone layer to the organic moss-humus layer, and therefore simultaneous high evaporation and high water table can create large differences between the

moisture contents of the two layers (Fig. 5D,E,G). The largest ~~errors in differences between data and~~ rootzone simulations are
390 ~~found~~ in mixed forested-peatland grid-cells (Fig 5F,G) mostly due to overestimation of the water table level ~~for the beginning~~
~~of the season.~~

~~Comparison of SpaFHy-2D simulated and in-situ observed groundwater levels is given in the Supplement (see Fig. S7)~~
~~in early summer.~~ Considering that no ~~model~~ calibration was conducted, ~~water table levels were simulated relatively well.~~
~~Particularly, the comparison of SpaFHy-2D simulated and in-situ observed groundwater levels show rather good model performance,~~
395 ~~and particularly~~ the shallow water tables are well captured ~~but also~~ (see Fig. S5 and Table S4). As we aim to assess the influence
~~of lateral flow on shallow soil moisture dynamics rather than fully replicate the observations, the performance of the 2D model~~
~~is considered sufficient.~~

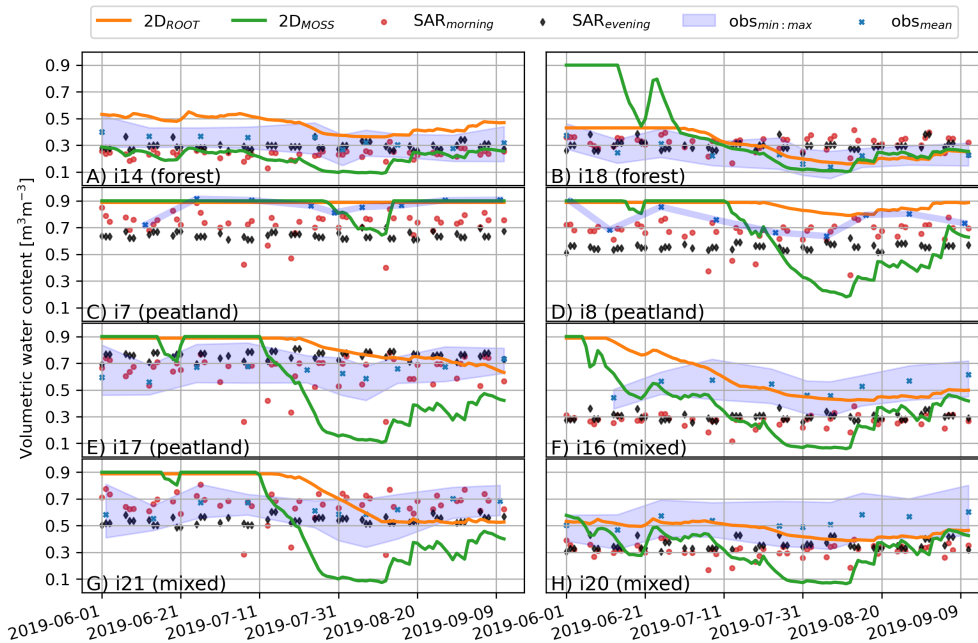
~~SAR-based shallow soil moisture mostly fall within the observed range, and the SAR morning flyover captures main~~
~~temporal dynamics of the observations, particularly drying in June and wetting in late August (Figs. 4 and 5). However, the~~
400 ~~SAR-based estimates consistently fall short of the highest observed and simulated values, leading to an underestimation of soil~~
~~moisture content (Fig. 5). There is also noticeable noise in SAR-based soil moisture, and the level and temporal patterns of SAR~~
~~morning and evening flyovers differ from each other. The comparison at different locations (Fig. 5: two forest, three peatland,~~
~~and three mixed forested-peatlands grid-cells~~~~with deeper water table levels agree reasonably well.)~~ shows a systematic shift
~~(up to $0.2 \text{ m}^3 \text{ m}^{-3}$) between SAR morning and evening flyover.~~

405 3.3 ~~Effect of groundwater flow conceptualizations~~

~~Scatterplots of simulated rootzone moisture content by 1D, TOP and 2D SpaFHy versions (see Sect. 2.2) and SAR-based~~
~~estimates against in-situ spatiotemporal soil moisture observations (see Sect. 2.5)~~

3.3 Effect of groundwater flow conceptualizations on soil moisture

~~The in-situ soil moisture data is further used to compare the model conceptualizations and to assess the impact of groundwater~~
410 ~~flow on shallow soil moisture~~ across the catchment ~~are shown in~~ (Fig. 6.~~The~~). ~~The comparison shows that the~~ observed soil
moisture ~~contents~~ below ca. $0.55 \text{ m}^3 \text{ m}^{-3}$ are rather well captured by all model conceptualizations ~~(Fig. 6A,B,C), especially~~
~~considering the uncertainties in soil hydraulic parameters based on geospatial data (Fig. 2: soil type).~~ Most of the forest grid-
cells (i.e. grid-cells with high canopy fraction) belong to this category. The results indicate model performance improves when
the lateral flows are accounted for, and only the 2D approach with explicit lateral groundwater flow can satisfactorily reproduce
415 the wetter conditions above $0.55 \text{ m}^3 \text{ m}^{-3}$, commonly found on open peatland grid-cells, and occasionally on forest grid-cells
~~(Fig. 6).~~ Conceptually, the SpaFHy-TOP should also be able to mimic groundwater dynamics via TWI. However, it ~~is~~ ~~was~~
able to capture only one of the observed wet grid-cells, and the overall goodness-of-fit ~~metrics are~~ ~~is~~ close to the SpaFHy-
1D version. All evaluation metrics are considerably better for the 2D model, but ~~it~~ ~~this model variant~~ tends to overestimate
soil moisture on ~~the~~ peatland grid-cells, consistent with ~~the overestimation in~~ Fig 5F,G. ~~In contrast to the models, SAR-based~~
420 ~~estimates have low correspondence with the observed soil moisture when canopy fraction is high, but match the observations~~
~~better than the model on open and wetter grid-cells (i.e. peatlands)~~



Temporal dynamics of

SpaFH_y-2D simulated, SAR-estimated and *in-situ* measured soil moisture at two forest, three peatland and three mixed forested peatland locations during June–Sept period in 2019.

Figure 5. Temporal dynamics of SpaFH_y-2D simulated, SAR-estimated and *in-situ* measured range of soil moisture ($obs_{min:max}$) at two forest, three peatland and three mixed forested peatland locations during June–Sept period in 2019.

The same comparison, but with colors classifying the points as either mineral soil or peat soil (based on Fig. 2: soil type) in Fig. S6C indicates that many of the grid-cells where model overestimates soil moisture are either faultily parameterized as peat soil, or the model may exaggerate the impact of lateral flow at those locations. However, it is worth noting that the observations include all measurements in the rootzone (0–30 cm), surpassing the assumed penetration depth of the SAR signal (1–5 cm).

425

Qualitative spatial evaluation of the three model versions was conducted against data from the two measurement campaigns in 2021 (model versions in Fig. 7). Common to all model variants, reveals that the large-scale spatial heterogeneity of shallow soil moisture is most strongly driven by the soil type (see Fig. 2) via the soil hydraulic properties. Particularly the differences in the 1D simulation come arise almost solely from differences in soil types (coarse and medium texture mineral soil and peat), while the role of vegetation heterogeneity was minimal, appears minimal (Fig. 10). The histograms of 1D simulations reveal that the show that daily moisture values are distributed around field capacities of mineral and peat soils. This is also (Fig. 7), consistent in Fig. S3–S7A where all daily simulated distributions are shown. All model conceptualizations match rather well the drier observations in the upland forest areas rather well, consistent with Fig. 6. However, as the 1D approach assumes independent grid-cells and neglects groundwater storage and flow, the soil moisture estimates do not reach the observed high values as drainage rapidly removes water excessive to field capacity. Hence, the 1D simulation is biased low at wet locations

435

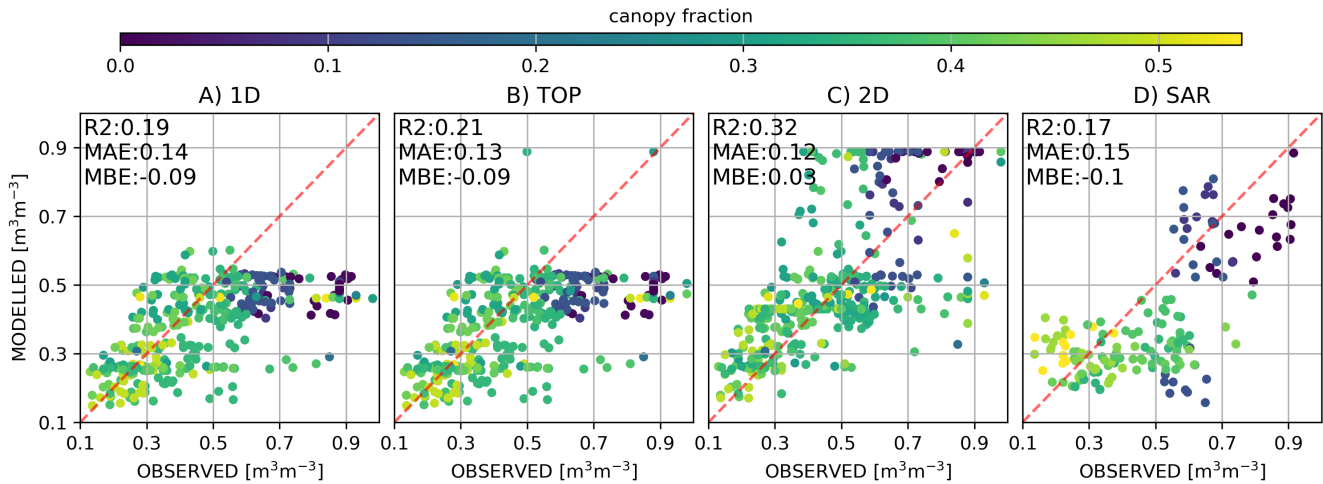


Figure 6. Comparison of simulated rootzone soil moisture content and SAR-based surface soil moisture estimates against spatiotemporal manual *in-situ* soil moisture observations. The color of the points correspond to grid-cell canopy fraction, ranging from open peatlands to forest grid-cells.

(see e.g. peatlands Figs. 6 and 7). Slightly more spatial variability can be seen in the TOP simulation, as it accounts for the return flow from the conceptual groundwater storage into the rootzone. Yet, the cells where return flow groundwater storage is activated remain rare (except close the stream network) even in wet conditions (2021-06-17, Fig. 7B) and almost non-existent in drier autumn conditions (2021-09-01), leading to a poor match between the model predictions and observations in wet locations. Fig. 7E).

The 2D model version SpaFHy-2D simulates larger saturated areas and match most of the point observations well in Fig. 7. Nevertheless, there are still inaccuracies, as saturated conditions adjacent to ditches are not well simulated, and the observed variability in the forest forests is not fully captured. The spatial variability of soil moisture in the 2D simulation depends strongly on the water table dynamics. Compared to other model variants, this creates stronger soil moisture variability within the catchment and yields better agreement with the observations. The histograms of Fig. 7C,F and Fig. S3-S7C also show higher frequency for grid-cells to be wet.

3.4 Comparison of SpaFHy-2D and SAR-based estimates spatial soil moisture

Comparison against the available point-scale observations

Previous section suggests that it is necessary to include the lateral groundwater flow to model the spatial patterns of soil moisture at LJO catchment. Point-scale However, comparison to point measurements can only capture a fraction of the simulated time steps and grid-cells, and thus, a comparison with the spatially explicit SAR-based soil moisture is conducted in useful. In contrast to the model, SAR-based soil moisture have poorer correspondence with the observations in grid-cells where

canopy fraction is high, but provide better match on open and wetter grid-cells (i.e. peatlands, Figs. 6D and S6D). However, it
455 is worth noting that the observations in Figs. 6D and S6D include all measurements in the rootzone (0–30 cm), surpassing the
assumed penetration depth of the SAR signal (1–5 cm).

A spatial comparison between SpaFHy-2D and spatially explicit SAR-based soil moisture is shown in Fig. 8. As already
noted, the simulated spatial patterns ~~follow mostly the~~ mostly follow soil parameterizations, as well as water table dynamics
affected by the lateral flow. The vegetation heterogeneity and consequent differences in rainfall interception and evaporation
460 result in additional variability for simulated organic moss-humus layer moisture in dry conditions (~~see also Fig. 5~~ Figs. 5 and
10). SAR and the SpaFHy-2D rootzone simulations agree on their main spatial patterns (i.e. drier forests and wetter peatlands).
~~However, it is~~ A spatiotemporal comparison metrics (Table S5) show that SAR generally predicts lower mean soil moisture
and variance (mean, variance = 0.34, 0.02 m³m⁻³) than SpaFHy-2D (mean, variance = 0.39, 0.04 m³m⁻³), but higher mean
soil moisture and variance compared to SpaFHy-1D (mean, variance = 0.29, 0.01 m³m⁻³). It is also noticeable from Table S5
465 that the wet quantiles (0.9) of SpaFHy-2D rootzone (0.82 m³m⁻³) and SAR (0.65 m³m⁻³) both suggest a major influence of
lateral groundwater flow on soil moisture, consistent with earlier findings concerning peatlands (Fig. 8) throughout the season
(Fig. 5C,D)

It is likely that SpaFHy-2D overestimates organic moss-humus layer moisture content variability, as there is a clear dis-
crepancy between the SpaFHy-2D and the SAR-based estimates. The simulations provide too high moisture content in wet
470 (Fig. 98A) and are biased low in drier conditions (Fig. 9D) ~~conditions~~ 8D). Compared to the simulations, SAR data shows
significantly more cell-to-cell variability and the histogram appears nearly normally distributed, especially below 0.55 m³m⁻³
(mainly mineral soils). Histograms of all daily soil moisture values in Fig. S3-S7D confirm that the SAR data tends to be nor-
mally distributed between 0.1 and 0.5 m³m⁻³. A closer look at the rectangular box shown in Fig. 8 further confirms the good
agreement of SpaFHy-2D -simulated and SAR-estimated rootzone moisture both at the dry and wet areas, but also demonstrates
475 the high cell-to-cell variability in SAR-based soil moisture (Fig. 9).

Considering the ability of SAR to relatively well predict peatland soil moisture (~~Fig. 6~~ Figs. 6D and S6D), the agreement
of SpaFHy-2D and SAR provide support for ~~the our~~ our earlier findings that soil moisture predictions improve when the lateral
groundwater flow is included (SpaFHy-2D). ~~A closer look at the rectangular box shown in Fig. 8 further confirms the good~~ The
agreement of SpaFHy-2D ~~-simulated and SAR-estimated rootzone moisture both at the dry and wet areas, but also highlights~~
480 ~~the high cell-to-cell variability in SAR-based soil moisture~~ and SAR is further supported by a quantitative comparison in
Fig. S8, where two clusters of soil moisture emerge in peatlands. The cluster of wet points correspond to the grid-cells with
groundwater flow influence, while the other cluster is not impacted by the lateral flow. The consistency between the SAR
and SpaFHy-2D is not as clear on mineral soil grid-cells (Fig. S8), likely due to uncertainties in the model's soil hydraulic
parameters as well as limitations in SAR soil moisture detection in forests (Fig. 96).

485 3.5 Drivers of spatiotemporal soil moisture variability

To better separate the role of lateral groundwater flow ~~and water table dynamics~~ from that of vegetation heterogeneity under
different temporal soil moisture regimes, Fig. 10 shows the grid-cell to grid-cell differences ($\Delta\theta$) between SpaFHy-2D and 1D

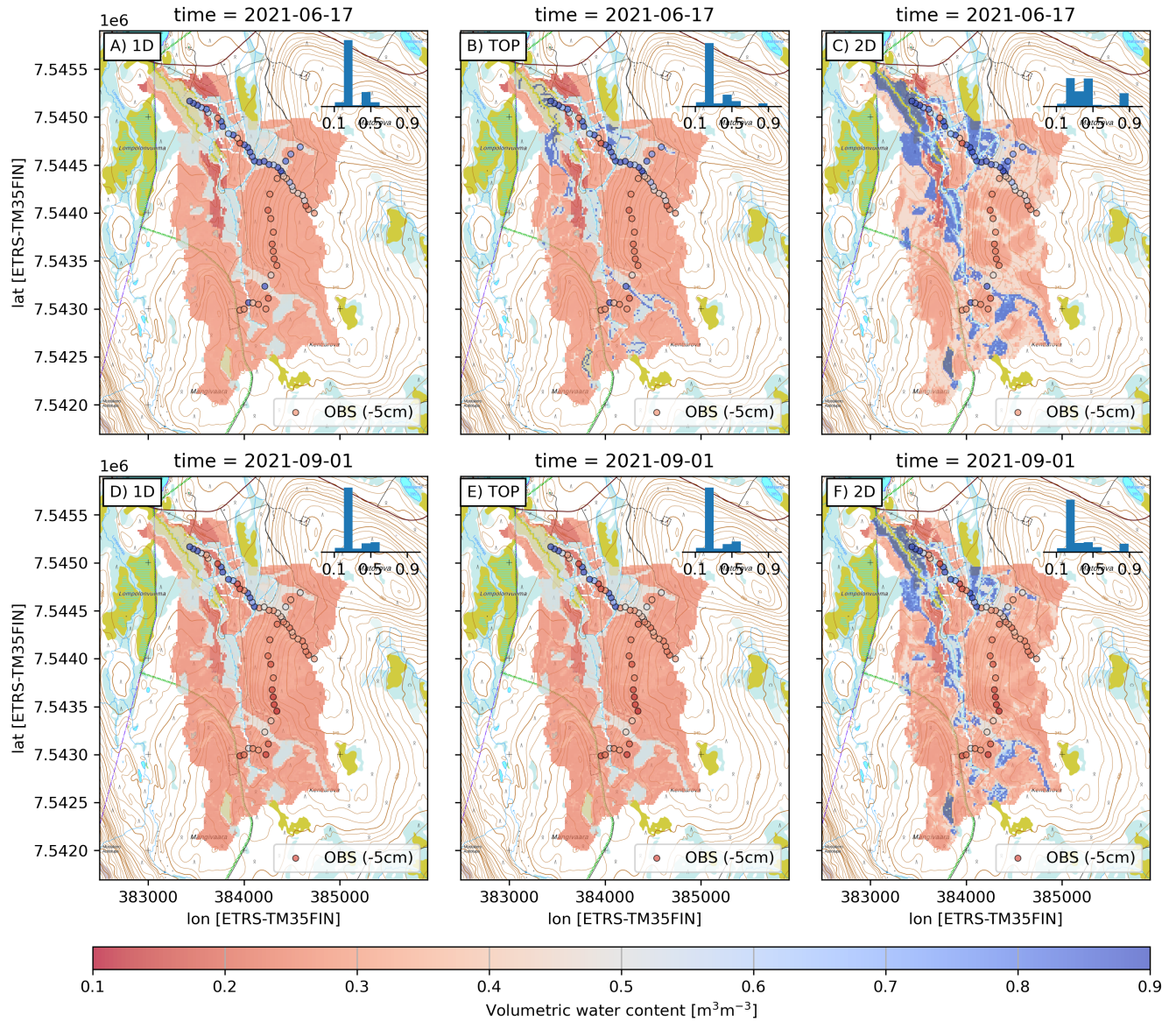


Figure 7. Spatial ~~patterns~~ patterns of modeled rootzone volumetric water content by the three model conceptualizations on 2021-06-17 (upper row, more moist) and 2021-08-01 (lower row, drier conditions). The bar plot shows binned distributions of simulated grid-cell soil moisture across the whole catchment, and ~~in-situ~~ in-situ measurements at 5 cm depth are shown as circles. The rasters overlay a topographic map (NLSF, 2020).

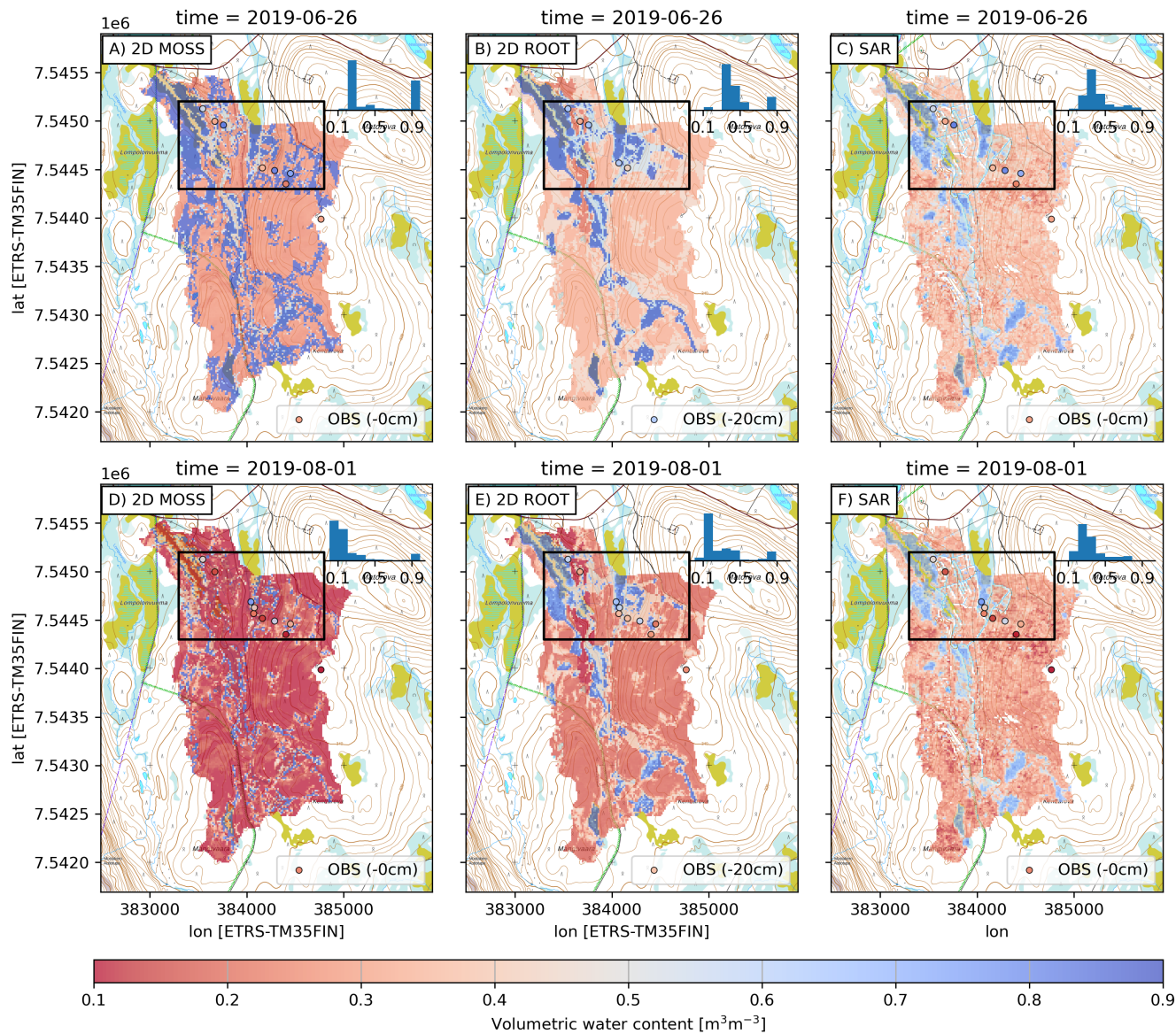


Figure 8. Spatial ~~patterns~~patterns of SpaFHy-2D modeled rootzone and organic moss-humus moisture, and SAR-based estimates on wet (2019-06-26, upper row) and dry day (2019-08-01, lower row). ~~In-situ~~In-situ measurements at 0 cm and 20 cm depths are shown as circles, and the bar plot shows binned distributions of simulated and SAR-estimated soil moisture across the whole catchment. The rectangular box shows an area that is presented in Fig. 9. The rasters overlay a topographic map (NLSF, 2020).

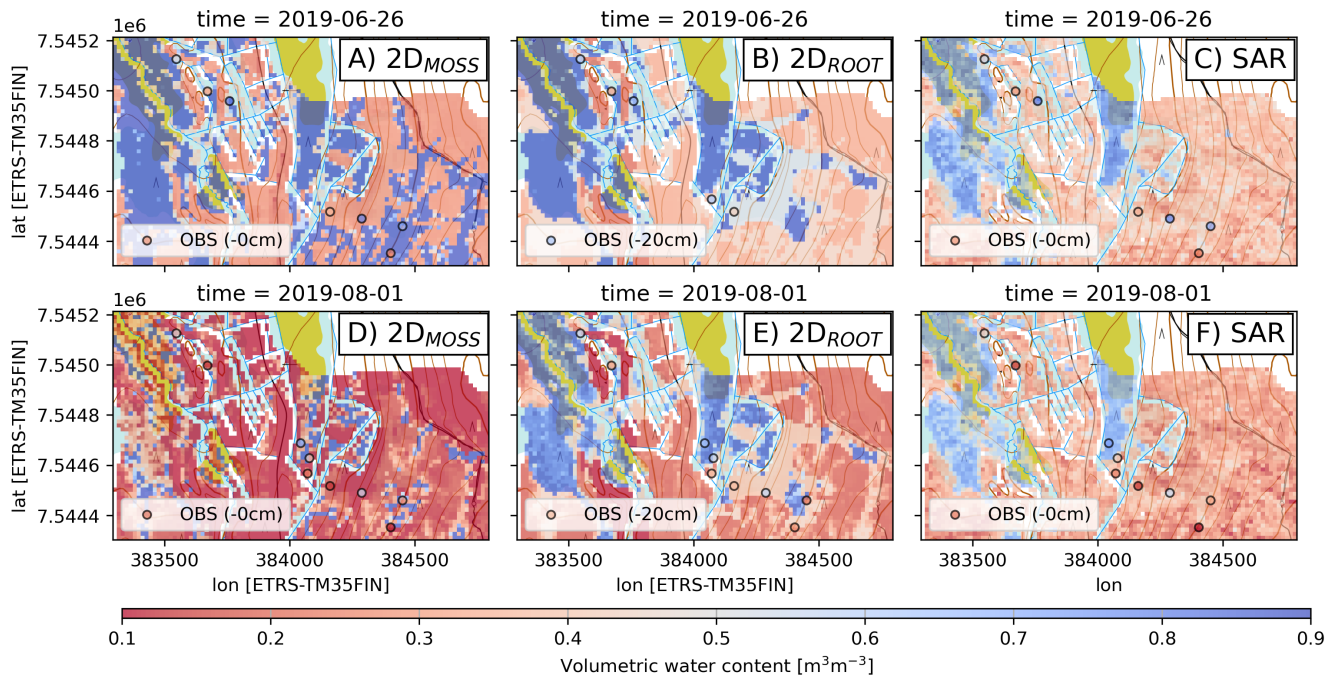


Figure 9. A zoomed in distribution of 2D modeled rootzone and organic moss-humus moisture and SAR-based estimates on wet (2019-06-26, upper row) and dry day (2019-08-01, lower row). *In-situ-In-situ* measurements at 0 cm and 20 cm depths are shown as circles. The rasters overlay a topographic map (NLSF, 2020).

simulations as well as between 1D and 1D_{homog.canopy} runs. ~~The dry to wet conditions are represented by quantiles of 0.1, 0.5 and 0.9 of grid-cell rootzone soil moisture content.~~ As expected, the difference between SpaFHy-2D and 1D simulations is
 490 highest in wet conditions. ~~In the wettest conditions~~ (q = 0.9, Fig. 10C). ~~In this case~~ the lateral groundwater flow has a large impact on soil moisture (mean $\Delta\theta$ between 2D and 1D ca. $0.1 \text{ m}^3\text{m}^{-3}$) ~~and~~ in major part of the catchment, including also parts of the forested areas. The difference between the models is smallest at periods with intermediate soil moisture (q = 0.5, mean difference ca. $0.05 \text{ m}^3\text{m}^{-3}$, Fig. 10B) ~~when the differences emerge,~~ during which the lateral flow has an effect almost only in peatland grid-cells. Interestingly, the difference between the 2D and 1D predicted soil moisture ~~is~~ becomes
 495 also in dry conditions (mean difference ca. $0.07 \text{ m}^3\text{m}^{-3}$, Fig. 10A), indicating a long-lasting effect of lateral groundwater flow from the upland to the lowland grid-cells. The role of vegetation heterogeneity on soil moisture patterns is negligible at intermediate and wet conditions (Fig. 10E,F), and only minor differences are found in very dry conditions (Fig. 10D). The vegetation heterogeneity plays a larger role in the moisture content of the organic moss-humus layer, but the impact of lateral flow still remains stronger (Fig. S6S9).

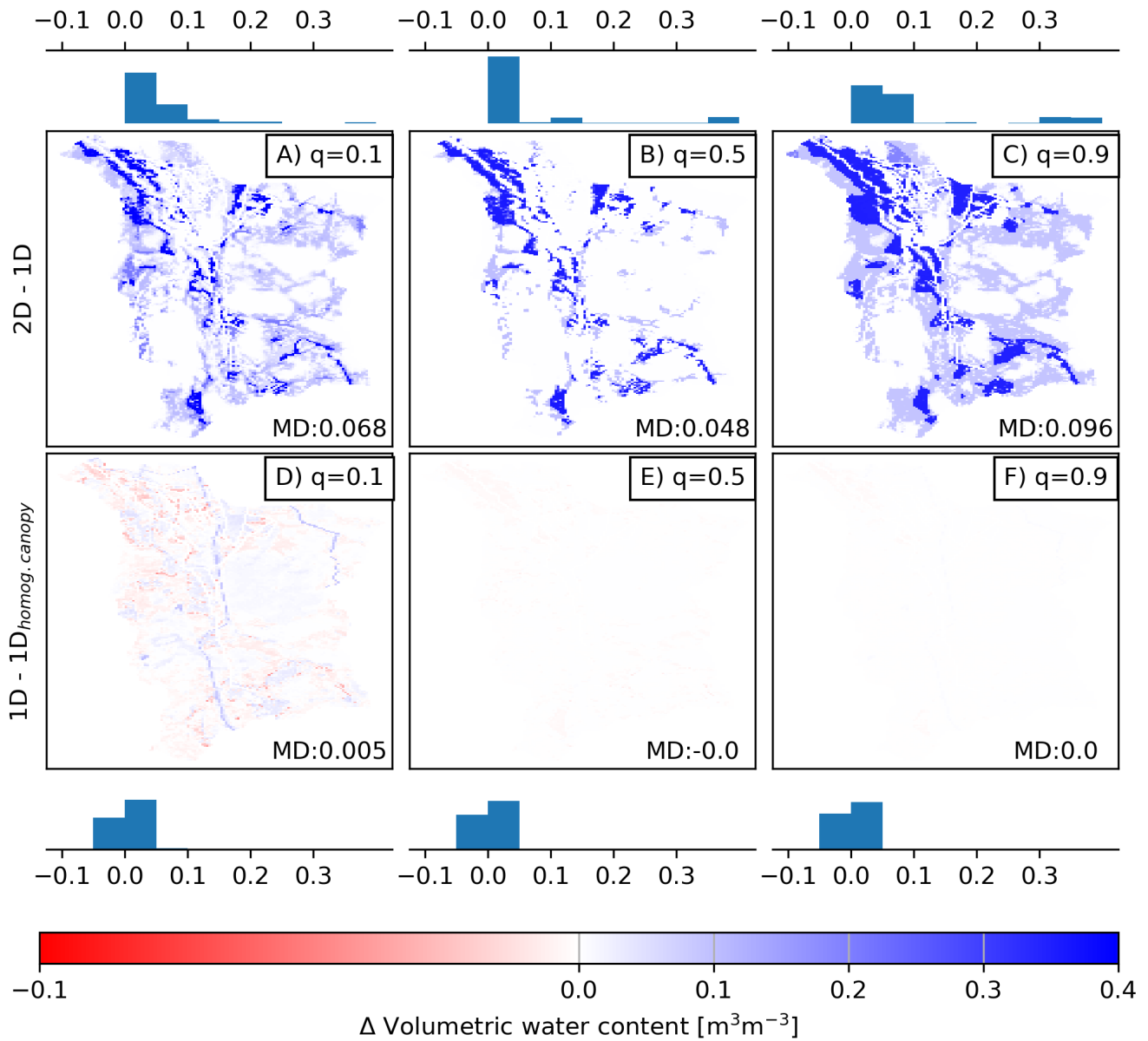


Figure 10. The impact of lateral groundwater flow (upper row) on rootzone soil moisture expressed as $\Delta\theta = 2D - 1D$, and the impact of vegetation heterogeneity (bottom row) expressed as $\Delta\theta = 1D - 1D_{homog.canopy}$ in different catchment soil moisture states. The panels correspond to 0.1, 0.5, and 0.9 quantiles of grid-cell soil moisture, and the bars show distribution of binned differences. Mean difference (MD) is shown in each panel. Note that blank panel refers to $\Delta\theta = 0.0 \text{ m}^3\text{m}^{-3}$.

4.1 Insights on the role of lateral groundwater flow for ~~top-shallow~~ soil moisture

Our multi-scale data and high-resolution process-based simulations in the subarctic LJO catchment showed that regardless of the catchment hydrologic state (from ~~very dry to very wet conditions~~ dry summer to very moist conditions after snowmelt), lateral groundwater flow plays a major role in shaping the spatial variability ~~and dynamics~~ of soil moisture (Fig. 10). The results indicate that spatially resolved models, which include groundwater flow are necessary to ~~reliably predict the~~ predict soil moisture variability at high-latitude catchments. Nevertheless, ~~explicit description of~~ lateral groundwater flow is commonly neglected in current hydrological and land surface models that operate at a coarse resolution (Best et al., 2011; Lawrence et al., 2012; Niu et al., 2011; Noilhan and Mahfouf, 1996). Increasing the spatial resolution of hydrological and biogeochemical land-surface models is the current trend; for instance Wood et al. (2011) set the ambition for future hyper-resolution LSMs to ~~simulate at horizontal resolutions of~~ 1 km for global-scale and 100 m for regional-scale simulations. When the models are adapted to finer grids, it becomes increasingly important to implement ~~processes describing lateral groundwater flows~~ lateral groundwater dynamics (Ji et al., 2017; Kim and Mohanty, 2016; Decker et al., 2013). Our relatively simple 2D shallow groundwater Darcy flow model, incorporating only 7 additional parameters (water retention parameters, ~~soil depth to bedrock~~, and stream water level) ~~which were~~ determined using openly available digital elevation model, soil type and stream network rasters, performed comparably to the state-of-the-art integrated surface-groundwater model HydroGeoSphere (Brunner and Simmons, 2012) in predicting observed groundwater levels at the LJO catchment (~~see Fig. S7 and compare Fig. S6 and Table S4 in our Supplement, and Fig. 6 and Table S6 in~~ Autio et al. (2023)). Also, the ~~simulation of~~ groundwater influenced areas in the catchment ~~is~~ are in broad agreement with the simulations by Autio et al. (2023).

Regardless of the known sensitivity of ecohydrological fluxes (i.e. interception, evaporation, transpiration) to changes in LAI and plant type (Launiainen et al., 2019; Kozii et al., 2020; Launiainen et al., 2016), the impact of lateral groundwater flow outweighed the impact of vegetation heterogeneity on soil moisture dynamics throughout the year. However, ~~it is worth noting that~~ the growing season in Pallas is ~~rather short~~, short and vegetation rather sparse and not very heterogeneous within the site classes (Fig. 2). In addition, the impact of vegetation heterogeneity on soil moisture is attenuated due to the compensating processes; soil evaporation decreases while transpiration and interception evaporation increase with increasing LAI, resulting in less drastic changes in total ET (Leppä et al., 2020; Launiainen et al., 2019). Consistent with Kollet and Maxwell (2008), the impact of groundwater flow on ~~top-shallow~~ soil moisture persisted also in dry conditions, suggesting high resilience of ~~low-lying eells~~ lowlands to droughts due to long-lasting lateral flow from the upland ~~eells~~ part of the catchment. The simulations showed that ~~at for~~ large parts of the catchment, ~~rootzone~~ moisture content was controlled by lateral groundwater flow, and the strength of ~~the~~ this effect depends on the state of the groundwater storage. Ji et al. (2017) showed that the role of lateral ~~flux~~ water flow becomes crucial in high-resolution land surface simulations in a region dominated by a humid climate and coniferous forests in the western USA. At a resolution of 100 meters, they showed that subsurface lateral flow transports moisture from high elevation areas to valley bottoms, impacting local grid-cell and catchment average ET especially in dry conditions. Kollet and

Maxwell (2008) coupled a groundwater and a land surface model, and demonstrated that when the water table depth was above
535 5 meters, there was strong coupling between groundwater dynamics and land surface processes at the subhumid grassland-
dominated watershed in the USA. Our results at LJO catchment are in line with these studies [regarding the importance of
groundwater flow on shallow soil moisture](#).

The impact of lateral flow was found especially important for peatlands, both due to the high porosity of peat (Menberu
et al., 2021) and location in the valley bottom ([FigFigs. 2, 7 ,and 8](#)). Mineral forest top soils can also be (temporarily) impacted
540 by lateral flow, especially [during heavy precipitation and snow melt, but soon after strong precipitation events and snowmelt](#).
[However](#), the difference between 1D and 2D models remained smaller due to the small difference in mineral soil field capacity
and porosity (Fig. 10).

4.2 SAR-based soil moisture: Potential and limitations

The Sentinel-1 SAR-based soil moisture estimates were useful to supplement the point-scale ~~in-situ~~ [in-situ](#) measurements
545 and confirm the plausibility of the spatial soil moisture predicted by the SpaFHy-2D. To this date, model developments and
evaluations of soil moisture predictions in boreal and subarctic forests and peatlands have been typically limited to point-
scale studies, which fails to encompass the full spatiotemporal extent that distributed hydrological models are simulating
(Launiainen et al., 2015; Ala-aho et al., 2017b; Tyystjärvi et al., 2022). We found SAR-estimates ~~very~~ useful for spatial model-
data comparison, and envision SAR to have further potential, for instance, as a proxy for water table depth assimilation or
550 improved estimates of topographic wetness indices (TWI, depth-to-water) in peatlands (Bechtold et al., 2020; Zhang et al.,
2018).

The comparison between SAR-based estimates and modeled soil moisture was not straightforward and revealed limita-
tions in using the SAR-based data, for instance as ground-truth calibration data for hydrological models. A direct comparison
is challenging due to the disparate penetration depth of SAR in soil (1–5 cm: Nolan and Fatland (2003)), contrasting with
555 the model layering (rootzone layer of 0–30 cm). Indeed, the correspondence of SAR-based estimates against ~~in-situ~~ [in-situ](#)
measurements in the rootzone (0–30 cm, Fig. 6) was poorer than the original validation of SAR-estimates against ~~in-situ~~
[in-situ](#) measurements at the surface soil (0 cm, Fig. 11 in Manninen et al. (2021)). [Enhancing This vertical mismatch is
a common challenge \(Shellito et al., 2020\), and hence, enhancing](#) the comparability of [in-situ](#) measurement as well as hy-
drological models with SAR-estimates would contribute to more effectively harnessing the SAR-based data. Another no-
560 table difference is that hydrological models ~~;~~ such as SpaFHy ~~;~~ [treat individual grid-cells homogeneously, neglecting neglect](#)
heterogeneity within the grid-cells, while SAR-estimates can integrate multiple backscattering signals for a given grid-cell
[\(Manninen and Jaaskelainen, 2021\)\(Manninen et al., 2021\)](#). In turn, hydrological models can integrate temporal information,
whereas SAR-based estimates are instantaneous.

We also emphasize the need for potential algorithm improvements in computing soil moisture from SAR signals. Given the
565 homogeneity of the vegetation and soil texture, some of the spatial variability in the SAR-based data appeared more as noise
than realistic soil moisture patterns. ~~SAR-estimated temporal dynamics were weak and partly hidden under the noise.~~ The
different SAR incidence and view angles with respect to the topography, to a large extent, cause the systematic difference of

the soil moisture estimates from the morning and evening flyover times (Fig. 4, Fig. Figs. 4 and 5). ~~The~~ ~~Indeed~~, topography-induced shading ~~was markedly more challenging~~ ~~posed a significant challenge~~ for the development of the evening soil moisture algorithm ~~of~~ ~~for~~ SAR-based estimates (Manninen et al., 2021). ~~The~~ ~~Consequently~~, Manninen et al. (2021) reported higher RMSEs for the evening ($0.088 \text{ m}^3 \text{ m}^{-3}$) than for the morning flyover ($0.065 \text{ m}^3 \text{ m}^{-3}$) while the maximum errors were relatively similar ($0.341 \text{ m}^3 \text{ m}^{-3}$ for morning and $0.339 \text{ m}^3 \text{ m}^{-3}$ for evening flyover). Further discussion on the differences between these SAR flyovers can be found in Manninen et al. (2021).

Although the SAR-based soil moisture fell mostly within the observed range, the temporal variability and seasonal patterns, especially from the evening flyovers, were small and followed neither the simulated nor *in-situ* observed shallow soil moisture (Fig. 5). The morning flyover occasionally captured some temporal dynamics observed and simulated (see e.g. Fig. 5D). The SAR-based estimates do not reach the highest observed or simulated values, resulting in underestimation of the soil moisture content, likely because they integrate information from multiple signals within a given grid-cell that have been averaged to correspond to the model grid. The presence of different vegetation characteristics and soil textures further complicates the interpretation of the backscattering signals, leading to uncertainties and noise in soil moisture estimates.

Overall, the capability of any remote sensing based soil moisture estimate to represent various meteorological and landscape conditions can only be as good as the training data. As acquiring high quality and representative *in-situ* ~~in-situ~~ soil moisture data is challenging and costly, we encourage deeper collaboration between hydrological measurements, modeling and remote sensing communities.

585 4.3 Model limitations and outlook

The modularity of SpaFH_y (Launiainen et al., 2019) was ideal for comparing the impact of different conceptualizations of the lateral groundwater flow. Nevertheless, there are potentially relevant hydrological processes that are not yet represented. For instance, overland flow and soil freezing and thawing are currently omitted, and this may influence soil moisture dynamics, particularly during and after snowmelt and in the autumn (Ala-Aho et al., 2021). Lateral overland flow has been found to distribute water from saturated grid-cells to unsaturated areas (e.g. in subarctic tundra and boreal forests; Tang et al., 2014). We suspect that it may be especially important after snowmelt and heavy precipitation events on the low-lying flat peatlands of the catchment. The snowpack representation of SpaFH_y successfully captured the snowmelt timing (Fig. S1, S4 Figs. S2 and S3), but relies on a simple degree-day approach, potentially limiting its ability to fully capture snowmelt dynamics. Moreover, the radiation conditions on the forest floor within a specific grid-cell may be influenced by the ~~surrounding forest canopy outside~~ ~~that grid-cell~~ forest canopy in the surroundings. Thus, employing 3D radiation transfer schemes that consider the shading from grid-cell neighbours (Webster et al., 2023), or the demography of individual trees within a grid-cell could be beneficial (Mazzotti et al., 2021). ~~Although the~~

Although the explicit 2D lateral groundwater flow module added process realism and significantly improved soil moisture simulations, it improved shallow soil moisture predictions, the simulations were still far from perfect, due to uncertainties in classifying soil types and because soil moisture data was not used to calibrate the model's hydraulic parameters. The improvement also comes with a computational cost; in terms of running time, SpaFH_y-2D is approximately sixty times

slower than TOP and 1D versions. For instance, a one-year simulation with 1D and TOP was completed in 5.4 seconds, while 2D took 321.6 seconds. This can become a burden when applying the 2D model to large areas, or when parameter calibration is needed or ensemble simulations are done.

605 Uncertainties in model simulations and model evaluation accumulate from multiple sources: input data, model parameters, model structure and errors in *in-situ* measurements (Moges et al., 2021). The meteorological forcing timeseries was constructed from observations at the upland forest site, and radiation data gaps were filled with ERA5 data (Hersbach et al., 2020). It is known that there are intrinsic uncertainties in meteorological observations (Stuefer et al., 2020). Although data gaps were limited, those filled by ERA5 data further add uncertainties in the model-data comparison (Raleigh et al., 2015). In addition, 610 we used spatially uniform meteorological forcing (excluding radiation where topographic shading was accounted for) measured at the forest site that may have been slightly different to those experienced on the lowland peatlands (Aurela et al., 2015).

 The model was initiated and parameterized based on the best available open geospatial data on the landscape characteristics. As Härkönen et al. (2015) found a good agreement between the mNFI-based and ground-based LAI estimates, and soil moisture patterns were not majorly altered by vegetation characteristics (Fig. 10), we assume that vegetation parameters did not create 615 marked biases in the soil moisture predictions. However, estimating soil hydraulic properties from available geospatial datasets is challenging (Launiainen et al., 2022) and can yield systematic uncertainties and biased local soil moisture. Modeling lateral groundwater flow by the proposed 2D Darcy scheme also requires distributed data on depth-to-bedrock. As such information was not readily available, these parameters were assigned as estimates. Even with these limitations, the modeled groundwater level dynamics were relatively close to the observed levels (Fig. S5 and Table S4)

620 5 Conclusions

We explored the controls of high-resolution soil moisture dynamics, particularly the role of lateral groundwater flow, in the sub-arctic Lompolojängänoja catchment in northwestern Finland. We combined soil moisture data from multiple sources, including in-situ in-situ measurements and Sentinel-1 SAR-based estimates, and interpreted soil moisture variability with high-resolution (16 × 16 m²) process-based hydrological modeling. To accomplish this, we extended the Spatial Forest Hydrology (SpaFH_y) 625 model with an explicit lateral groundwater (2D Darcy flow) submodel, and compared it to existing approaches where lateral groundwater flow was either neglected (free drainage) or based on a simple TOPMODEL conceptualization. The results showed the major impact of lateral groundwater flow in shaping soil moisture dynamics, particularly post snowmelt and after heavy rainfall. The inclusion of the lateral groundwater flow model notably improved soil moisture simulations in forested peatlands and open peatlands. The soil moisture simulations were affected by uncertainties in hydraulic parameters, which 630 were assigned based on geospatial data on soil types. SAR-based soil moisture estimates were valuable in confirming modeled spatial patterns. Discrepancies in spatial resolutions, SAR penetration depth, and model layering, however, hampered direct comparison. Moreover, the noise in SAR-based data, particularly under forested areas, complicates its use as ground-truth evaluation data for hydrological models. Our study provides novel insights and tools for predicting soil moisture dynamics at

high-resolution, necessary for ecohydrological, biogeochemical, and climate change adaptation studies, as well as for land-use
635 management and planning in high-latitude environments.

Code and data availability. SpaFHy model version developed and used in this study is available at Nousu et al. (2024a). The code repository also includes meteorological forcing files and geospatial input rasters.

In-situ hydrological measurement data, including soil moisture, evapotranspiration, groundwater levels, and specific discharge, are available at Nousu et al. (2024b).

640 *Author contributions.* JPN, SL, PA and HM designed the research. JPN led the study and performed the model experiments and data analysis, with scientific contributions of KL, SL, GM, HM, TM and PA. *In-situ* manual measurements were conducted by JPN and MK. JPN was responsible for writing the article, with contributions from all authors. MA and AL provided the energy flux data, and TM provided the SAR data. SL, HM, PA and AL were responsible for the funding acquisition.

Competing interests. The contact author has declared that none of the authors has any competing interests.

645 *Acknowledgements.* This work was funded by the Research Council of Finland (RCF) (ArcI Profi 4). Giulia Mazzotti was funded by the Swiss National Science Foundation (grant no. P500PN_202741). Samuli Launiainen and Jari-Pekka Nousu acknowledge the GreenFeed-Back project from the EU Horizon Europe Framework Programme for Research and Innovation (grant no. 101056921). Samuli Launiainen acknowledges the support of RCF (no. 356138 & 348102). Pertti Ala-aho was funded by the RCF Research Fellow grant (no. 347348). We acknowledge the Ministry of Transport and Communications through the Integrated Carbon Observing System (ICOS), ICOS Finland and
650 RCF (grant no. 308511). The authors would like to thank Emmihenna Jääskeläinen and Anna Autio for valuable discussions during this work. We also acknowledge the use of ChatGPT 3.5 (Open AI, <https://chat.openai.com>) to proofread parts of the paper.

References

- Ala-aho, P., Soulsby, C., Wang, H., and Tetzlaff, D.: Integrated surface-subsurface model to investigate the role of groundwater in headwater catchment runoff generation: A minimalist approach to parameterisation, *Journal of Hydrology*, 547, 664–677, <https://doi.org/10.1016/j.jhydrol.2017.02.023>, 2017a.
- Ala-aho, P., Tetzlaff, D., McNamara, J., Laudon, H., and Soulsby, C.: Using isotopes to constrain water flux and age estimates in snow-influenced catchments using the STARR (Spatially distributed Tracer-Aided Rainfall-Runoff) model, *Hydrology and Earth System Sciences Discussions*, pp. 1–38, <https://doi.org/10.5194/hess-2017-106>, 2017b.
- Ala-Aho, P., Autio, A., Bhattacharjee, J., Isokangas, E., Kujala, K., Marttila, H., Menberu, M., Meriö, L. J., Postila, H., Rauhala, A., Ronkanen, A. K., Rossi, P. M., Saari, M., Haghighi, A. T., and Klove, B.: What conditions favor the influence of seasonally frozen ground on hydrological partitioning? A systematic review, *Environmental Research Letters*, 16, <https://doi.org/10.1088/1748-9326/abe82c>, 2021.
- Ameray, A., Cavard, X., and Bergeron, Y.: Climate change may increase Quebec boreal forest productivity in high latitudes by shifting its current composition, *Frontiers in Forests and Global Change*, 6, 1–19, <https://doi.org/10.3389/ffgc.2023.1020305>, 2023.
- Aurela, M., Lohila, A., Tuovinen, J. P., Hatakka, J., Penttilä, T., and Laurila, T.: Carbon dioxide and energy flux measurements in four northern-boreal ecosystems at Pallas, *Boreal Environment Research*, 20, 455–473, 2015.
- Autio, A., Ala-Aho, P., Rossi, P. M., Ronkanen, A.-K., Aurela, M., Lohila, A., Korpelainen, P., Kumpula, T., Klöve, B., and Marttila, H.: Groundwater exfiltration pattern determination in the sub-arctic catchment using thermal imaging, stable water isotopes and fully-integrated groundwater-surface water modelling, *Journal of Hydrology*, 626, 130–142, <https://doi.org/10.1016/j.jhydrol.2023.130342>, 2023.
- Bauer-Marschallinger, B., Freeman, V., Cao, S., Paulik, C., Schaufler, S., Stachl, T., Modanesi, S., Massari, C., Ciabatta, L., Brocca, L., and Wagner, W.: Toward Global Soil Moisture Monitoring With Sentinel-1: Harnessing Assets and Overcoming Obstacles, *IEEE Transactions on Geoscience and Remote Sensing*, 57, 520–539, <https://doi.org/10.1109/TGRS.2018.2858004>, 2019.
- Beale, J., Waine, T., Evans, J., and Corstanje, R.: A Method to Assess the Performance of SAR-Derived Surface Soil Moisture Products, *IEEE Journal of Selected Topics in Applied Earth Observations and Remote Sensing*, 14, 4504–4516, <https://doi.org/10.1109/JSTARS.2021.3071380>, 2021.
- Bechtold, M., De Lannoy, G. J., Reichle, R. H., Roose, D., Balliston, N., Burdun, I., Devito, K., Kurbatova, J., Strack, M., and Zarov, E. A.: Improved groundwater table and L-band brightness temperature estimates for Northern Hemisphere peatlands using new model physics and SMOS observations in a global data assimilation framework, *Remote Sensing of Environment*, 246, 111–125, <https://doi.org/10.1016/j.rse.2020.111805>, 2020.
- Bergström, S.: The HBV model - its structure and applications, *Swedish Meteorological and Hydrological Institute, Norrköping*, 4, 1–33, 1992.
- Best, M. J., Pryor, M., Clark, D. B., Rooney, G. G., Essery, R. L. H., Ménard, C. B., Edwards, J. M., Hendry, M. A., Porson, A., Gedney, N., Mercado, L. M., Sitch, S., Blyth, E., Boucher, O., Cox, P. M., Grimmond, C. S. B., and Harding, R. J.: The Joint UK Land Environment Simulator (JULES), model description – Part 1: Energy and water fluxes, *Geoscientific Model Development*, 4, 677–699, <https://doi.org/10.5194/gmd-4-677-2011>, 2011.
- Beven, K. J. and Kirkby, M. J.: A physically based, variable contributing area model of basin hydrology, *Hydrological Sciences Bulletin*, 24, 43–69, <https://doi.org/10.1080/02626667909491834>, 1979.
- Bhattacharai, N. and Wagle, P.: Recent Advances in Remote Sensing of Evapotranspiration, <https://doi.org/10.3390/rs13214260>, 2021.

- Bonan, G. B.: Carbon and Nitrogen Cycling in North American Boreal Forests . I . Litter Quality and Soil Thermal Effects in Interior Alaska, *Biogeochemistry*, 10, 1–28, 1990.
- 690 Bond-Lamberty, B., Smith, A. P., and Bailey, V.: Temperature and moisture effects on greenhouse gas emissions from deep active-layer boreal soils, *Biogeosciences*, 13, 6669–6681, <https://doi.org/10.5194/bg-13-6669-2016>, 2016.
- Brunner, P. and Simmons, C. T.: HydroGeoSphere: A Fully Integrated, Physically Based Hydrological Model, *Groundwater*, 50, 170–176, <https://doi.org/https://doi.org/10.1111/j.1745-6584.2011.00882.x>, 2012.
- 695 Buermann, W., Parida, B., Jung, M., MacDonald, G. M., Tucker, C. J., and Reichstein, M.: Recent shift in Eurasian boreal forest greening response may be associated with warmer and drier summers, *Geophysical Research Letters*, 41, 1995–2002, <https://doi.org/https://doi.org/10.1002/2014GL059450>, 2014.
- Celik, M. F., Isik, M. S., Yuzugullu, O., Fajraoui, N., and Erten, E.: Soil Moisture Prediction from Remote Sensing Images Coupled with Climate, Soil Texture and Topography via Deep Learning, <https://doi.org/10.3390/rs14215584>, 2022.
- 700 Clark, M. P., Slater, A. G., Rupp, D. E., Woods, R. A., Vrugt, J. A., Gupta, H. V., Wagener, T., and Hay, L. E.: Framework for Understanding Structural Errors (FUSE): A modular framework to diagnose differences between hydrological models, *Water Resources Research*, 44, <https://doi.org/10.1029/2007wr006735>, 2008.
- Clark, M. P., Nijssen, B., Lundquist, J. D., Kavetski, D., Rupp, D. E., Woods, R. A., Freer, J. E., Gutmann, E. D., Wood, A. W., Brekke, L. D., Arnold, J. R., Gochis, D. J., and Rasmussen, R. M.: A unified approach for process-based hydrologic modeling: 1. Modeling concept, *Water Resources Research*, 51, 2498–2514, <https://doi.org/10.1002/2015WR017200.A>, 2015.
- 705 Corradini, C.: Soil moisture in the development of hydrological processes and its determination at different spatial scales, *Journal of Hydrology*, 516, 1–5, <https://doi.org/10.1016/j.jhydrol.2014.02.051>, 2014.
- Crow, W. T. and Yilmaz, M. T.: The auto-tuned land data assimilation system (ATLAS), *Water Resources Research*, 50, 371–385, <https://doi.org/10.1002/2013WR014550>, 2014.
- 710 Daly, E. and Porporato, A.: A review of soil moisture dynamics: From rainfall infiltration to ecosystem response, *Environmental Engineering Science*, 22, 9–24, <https://doi.org/10.1089/ees.2005.22.9>, 2005.
- De Lannoy, G. J. M., Bechtold, M., Albergel, C., Brocca, L., Calvet, J.-C., Carrassi, A., Crow, W. T., de Rosnay, P., Durand, M., Forman, B., Geppert, G., Giroto, M., Hendricks Franssen, H.-J., Jonas, T., Kumar, S., Lievens, H., Lu, Y., Massari, C., Pauwels, V. R. N., Reichle, R. H., and Steele-Dunne, S.: Perspective on satellite-based land data assimilation to estimate water cycle components in an era of advanced data availability and model sophistication, *Frontiers in Water*, 4, <https://doi.org/10.3389/frwa.2022.981745>, 2022.
- 715 Decharme, B., Delire, C., Minvielle, M., Colin, J., Vergnes, J. P., Alias, A., Saint-Martin, D., Séférian, R., Sénési, S., and Voldoire, A.: Recent Changes in the ISBA-CTRIP Land Surface System for Use in the CNRM-CM6 Climate Model and in Global Off-Line Hydrological Applications, *Journal of Advances in Modeling Earth Systems*, 11, 1207–1252, <https://doi.org/10.1029/2018MS001545>, 2019.
- Decker, M., Pitman, A. J., and Evans, J. P.: Groundwater constraints on simulated transpiration variability over Southeastern Australian forests, *Journal of Hydrometeorology*, 14, 543–559, <https://doi.org/10.1175/JHM-D-12-058.1>, 2013.
- 720 Deschamps-Berger, C., Cluzet, B., Dumont, M., Lafaysse, M., Berthier, E., Fanise, P., and Gascoïn, S.: Improving the Spatial Distribution of Snow Cover Simulations by Assimilation of Satellite Stereoscopic Imagery, *Water Resources Research*, 58, e2021WR030271, <https://doi.org/https://doi.org/10.1029/2021WR030271>, 2022.
- Dobriyal, P., Qureshi, A., Badola, R., and Hussain, S. A.: A review of the methods available for estimating soil moisture and its implications for water resource management, *Journal of Hydrology*, 458-459, 110–117, <https://doi.org/10.1016/j.jhydrol.2012.06.021>, 2012.
- 725

- Elumeeva, T. G., Soudzilovskaia, N. A., Daring, H. J., and Cornelissen, J. H.: The importance of colony structure versus shoot morphology for the water balance of 22 subarctic bryophyte species, *Journal of Vegetation Science*, 22, 152–164, <https://doi.org/10.1111/j.1654-1103.2010.01237.x>, 2011.
- Esri: ESRI Satellite (ArcGIS/World_Imagery), <https://www.arcgis.com/home/item.html?id=10df2279f9684e4a9f6a7f08febac2a9>, 2023.
- 730 Essery, R., Pomeroy, J., Parviainen, J., and Storck, P.: Sublimation of snow from coniferous forests in a climate model, *Journal of Climate*, 16, 1855–1864, [https://doi.org/10.1175/1520-0442\(2003\)016<1855:SOSFCF>2.0.CO;2](https://doi.org/10.1175/1520-0442(2003)016<1855:SOSFCF>2.0.CO;2), 2003.
- FMI: Finnish Meteorological Institute past weather observations, available at: <https://en.ilmatieteenlaitos.fi/download-observations>, 2021.
- GSF: Geological Survey of Finland, bedrock 1:200 000 and superficial deposits 1:20 000 and 1:50 000, available at: <https://hakku.gtk.fi/en>, 2020.
- 735 Gupta, H. V., Kling, H., Yilmaz, K. K., and Martinez, G. F.: Decomposition of the mean squared error and NSE performance criteria: Implications for improving hydrological modelling, *Journal of Hydrology*, 377, 80–91, <https://doi.org/https://doi.org/10.1016/j.jhydrol.2009.08.003>, 2009.
- Härkönen, S., Lehtonen, A., Manninen, T., Tuominen, S., and Peltoniemi, M.: Estimating forest leaf area index using satellite images: comparison of k-NN based Landsat-NFI LAI with MODISRSR based LAI product for Finland, *Boreal Environment Research*, 20, 181–
- 740 195, 2015.
- Hersbach, H., Bell, B., Berrisford, P., Hirahara, S., Horányi, A., Muñoz-Sabater, J., Nicolas, J., Peubey, C., Radu, R., Schepers, D., Simmons, A., Soci, C., Abdalla, S., Abellan, X., Balsamo, G., Bechtold, P., Biavati, G., Bidlot, J., Bonavita, M., De Chiara, G., Dahlgren, P., Dee, D., Diamantakis, M., Dragani, R., Flemming, J., Forbes, R., Fuentes, M., Geer, A., Haimberger, L., Healy, S., Hogan, R. J., Hólm, E., Janisková, M., Keeley, S., Laloyaux, P., Lopez, P., Lupu, C., Radnoti, G., de Rosnay, P., Rozum, I., Vamborg, F., Vil-
- 745 laume, S., and Thépaut, J. N.: The ERA5 global reanalysis, *Quarterly Journal of the Royal Meteorological Society*, 146, 1999–2049, <https://doi.org/10.1002/qj.3803>, 2020.
- Holmberg, M., Futter, M. N., Kotamäki, N., Fronzek, S., Forsius, M., Kiuru, P., Pirttioja, N., Rasmus, K., Starr, M., and Vuorenmaa, J.: Effects of changing climate on the hydrology of a boreal catchment and lake DOC - probabilistic assessment of a dynamic model chain, *Boreal Environment Research*, 19, 66–82, 2014.
- 750 Huttunen, J. T., Nykänen, H., Turunen, J., and Martikainen, P. J.: Methane emissions from natural peatlands in the northern boreal zone in Finland, Fennoscandia, *Atmospheric Environment*, 37, 147–151, [https://doi.org/10.1016/S1352-2310\(02\)00771-9](https://doi.org/10.1016/S1352-2310(02)00771-9), 2003.
- IPCC: Chapter 2: Land–climate interactions, *Climate Change and Land: an IPCC special report on climate change, desertification, land degradation, sustainable land management, food security, and greenhouse gas fluxes in terrestrial ecosystems*, pp. 131–248, 2019.
- Isoaho, A., Ikkala, L., Marttila, H., Hjort, J., Kumpula, T., Korpelainen, P., and Räsänen, A.: Spatial water table level modelling with
- 755 multi-sensor unmanned aerial vehicle data in boreal aapa mires, *Remote Sensing Applications: Society and Environment*, 32, 101 059, <https://doi.org/https://doi.org/10.1016/j.rsase.2023.101059>, 2023.
- Iwata, Y., Miyamoto, T., Kameyama, K., and Nishiya, M.: Effect of sensor installation on the accurate measurement of soil water content, *European Journal of Soil Science*, 68, 817–828, <https://doi.org/https://doi.org/10.1111/ejss.12493>, 2017.
- J.-P. Vergnes, B. D. and Habets, F.: Introduction of groundwater capillary rises using subgrid spatial variability of topography into, *Journal*
- 760 *of Geophysical Research*, pp. 6578–6595, <https://doi.org/10.1002/2014JD021573>.Received, 2014.
- Ji, P., Yuan, X., and Liang, X. Z.: Do Lateral Flows Matter for the Hyperresolution Land Surface Modeling?, *Journal of Geophysical Research: Atmospheres*, 122, 077–12, <https://doi.org/10.1002/2017JD027366>, 2017.

- Jokinen, P., Pirinen, P., Kaukoranta, J.-P., Kangas, A., Alenius, P., Eriksson, P., Johansson, M., and Wilkman, S.: Climatological and oceanographic statistics of Finland 1991–2020, Tech. rep., <http://hdl.handle.net/10138/336063>, 2021.
- 765 Joo, J. and Tian, Y.: Impact of Stream-Groundwater Interactions on Peak Streamflow in the Floods, <https://doi.org/10.3390/hydrology8030141>, 2021.
- Junttila, S., Campos, M., Hölttä, T., Lindfors, L., Issaoui, A. E., Vastaranta, M., Hyypä, H., and Puttonen, E.: Tree Water Status Affects Tree Branch Position, *Forests*, 13, <https://doi.org/10.3390/f13050728>, 2022.
- Kalliokoski, T., Pennanen, T., Nygren, P., Sievänen, R., and Helmisaari, H. S.: Belowground interspecific competition in mixed boreal
770 forests: Fine root and ectomycorrhiza characteristics along stand developmental stage and soil fertility gradients, *Plant and Soil*, 330, 73–89, <https://doi.org/10.1007/s11104-009-0177-9>, 2010.
- Kankare, V., Luoma, V., Saarinen, N., Peuhkurinen, J., Holopainen, M., and Vastaranta, M.: Assessing feasibility of the forest trafficability map for avoiding rutting – A case study, *Silva Fennica*, 53, 1–9, <https://doi.org/10.14214/sf.10197>, 2019.
- Karhu, K., Auffret, M. D., Dungait, J. A., Hopkins, D. W., Prosser, J. I., Singh, B. K., Subke, J. A., Wookey, P. A., Agren, G. I., Sebastià,
775 M. T., Gouriveau, F., Bergkvist, G., Meir, P., Nottingham, A. T., Salinas, N., and Hartley, I. P.: Temperature sensitivity of soil respiration rates enhanced by microbial community response., *Nature*, 513, 81–84, <https://doi.org/10.1038/nature13604>, 2014.
- Kemppinen, J., Niittynen, P., Rissanen, T., Tyystjärvi, V., Aalto, J., and Luoto, M.: Soil Moisture Variations From Boreal Forests to the Tundra, *Water Resources Research*, 59, e2022WR032719, <https://doi.org/10.1029/2022WR032719>, 2023.
- Kim, J. and Mohanty, B. P.: Influence of lateral subsurface flow and connectivity on soil water storage in land surface modeling, *Journal of
780 Geophysical Research: Atmospheres*, 121, 704–721, <https://doi.org/10.1002/2015JD024067>, 2016.
- Kløve, B., Ala-Aho, P., Bertrand, G., Gurdak, J. J., Kupfersberger, H., Kvarner, J., Muotka, T., Mykrä, H., Preda, E., Rossi, P., Uvo, C. B., Velasco, E., and Pulido-Velazquez, M.: Climate change impacts on groundwater and dependent ecosystems, *Journal of Hydrology*, 518, 250–266, <https://doi.org/10.1016/j.jhydrol.2013.06.037>, 2014.
- Koch, J., Demirel, M. C., and Stisen, S.: The SPAtial EFficiency metric (SPAEF): Multiple-component evaluation of spatial patterns for op-
785 timization of hydrological models, *Geoscientific Model Development*, 11, 1873–1886, <https://doi.org/10.5194/gmd-11-1873-2018>, 2018.
- Koivusalo, H. and Kokkonen, T.: Snow processes in a forest clearing and in a coniferous forest, *Journal of Hydrology*, 262, 145–164, [https://doi.org/10.1016/S0022-1694\(02\)00031-8](https://doi.org/10.1016/S0022-1694(02)00031-8), 2002.
- Kolari, P., Lappalainen, H. K., Hänninen, H., and Hari, P.: Relationship between temperature and the seasonal course of photosynthesis in Scots pine at northern timberline and in southern boreal zone, *Tellus, Series B: Chemical and Physical Meteorology*, 59, 542–552,
790 <https://doi.org/10.1111/j.1600-0889.2007.00262.x>, 2007.
- Kollet, S. J. and Maxwell, R. M.: Capturing the influence of groundwater dynamics on land surface processes using an integrated, distributed watershed model, *Water Resources Research*, 44, 1–18, <https://doi.org/10.1029/2007WR006004>, 2008.
- Korkiakoski, M., Määttä, T., Peltoniemi, K., Penttilä, T., and Lohila, A.: Excess soil moisture and fresh carbon input are prerequisites for methane production in podzolic soil, *Biogeosciences*, 19, 2025–2041, <https://doi.org/10.5194/bg-19-2025-2022>, 2022.
- 795 Kozii, N., Haahti, K., Tor-Ngern, P., Chi, J., Maher Hasselquist, E., Laudon, H., Launiainen, S., Oren, R., Peichl, M., Wallerman, J. r., and Hasselquist, N. J.: Partitioning growing season water balance within a forested boreal catchment using sap flux, eddy covariance, and a process-based model, *Hydrology and Earth System Sciences*, 24, 2999–3014, <https://doi.org/10.5194/hess-24-2999-2020>, 2020.
- Krinner, G.: Impact of lakes and wetlands on boreal climate, *Journal of Geophysical Research: Atmospheres*, 108, <https://doi.org/10.1029/2002jd002597>, 2003.
- 800 Kuusisto, E.: Snow accumulation and snowmelt in Finland, *PUBLICATIONS OF THE WATER RESEARCH INSTITUTE*, 55 edn., 1984.

- Lagergren, F. and Lindroth, A.: Transpiration response to soil moisture in pine and spruce trees in Sweden, *Agricultural and Forest Meteorology*, 112, 67–85, [https://doi.org/10.1016/S0168-1923\(02\)00060-6](https://doi.org/10.1016/S0168-1923(02)00060-6), 2002.
- Larson, J., Wallerman, J., Peichl, M., and Laudon, H.: Soil moisture controls the partitioning of carbon stocks across a managed boreal forest landscape., *Scientific reports*, 13, 14 909, <https://doi.org/10.1038/s41598-023-42091-4>, 2023.
- 805 Launiainen, S., Katul, G. G., Lauren, A., and Kolari, P.: Coupling boreal forest CO₂, H₂O and energy flows by a vertically structured forest canopy - Soil model with separate bryophyte layer, *Ecological Modelling*, 312, 385–405, <https://doi.org/10.1016/j.ecolmodel.2015.06.007>, 2015.
- Launiainen, S., Katul, G. G., Kolari, P., Lindroth, A., Lohila, A., Aurela, M., Varlagin, A., Grelle, A., and Vesala, T.: Do the energy fluxes and surface conductance of boreal coniferous forests in Europe scale with leaf area?, *Global Change Biology*, 22, 4096–4113, <https://doi.org/10.1111/gcb.13497>, 2016.
- 810 Launiainen, S., Guan, M., Salmivaara, A., and Kieloaho, A. J.: Modeling boreal forest evapotranspiration and water balance at stand and catchment scales: a spatial approach, *Hydrology and Earth System Sciences*, 23, 3457–3480, <https://doi.org/10.5194/hess-23-3457-2019>, 2019.
- Launiainen, S., Kieloaho, A. J., Lindroos, A. J., Salmivaara, A., Ilvesniemi, H., and Heiskanen, J.: Water Retention Characteristics of Mineral Forest Soils in Finland: Impacts for Modeling Soil Moisture, *Forests*, 13, <https://doi.org/10.3390/f13111797>, 2022.
- 815 Laurén, A., Palviainen, M., Launiainen, S., Leppä, K., Stenberg, L., Urzainki, I., Nieminen, M., Laiho, R., and Hökkä, H.: Drainage and stand growth response in peatland forests—description, testing, and application of mechanistic peatland simulator susi, *Forests*, 12, 1–23, <https://doi.org/10.3390/f12030293>, 2021.
- Lawrence, D. M., Oleson, K. W., Flanner, M. G., Fletcher, C. G., Lawrence, P. J., Levis, S., Swenson, S. C., and Bonan, G. B.: The CCSM4 Land Simulation, 1850–2005: Assessment of Surface Climate and New Capabilities, *Journal of Climate*, 25, 2240–2260, <https://doi.org/https://doi.org/10.1175/JCLI-D-11-00103.1>, 2012.
- 820 Leppä, K., Hökkä, H., Laiho, R., Launiainen, S., Lehtonen, A., Mäkipää, R., Peltoniemi, M., Saarinen, M., Sarkkola, S., and Nieminen, M.: Selection Cuttings as a Tool to Control Water Table Level in Boreal Drained Peatland Forests, *Frontiers in Earth Science*, 8, 1–16, <https://doi.org/10.3389/feart.2020.576510>, 2020.
- 825 Li, F., Kurtz, W., Hung, C. P., Vereecken, H., and Hendricks Franssen, H. J.: Water table depth assimilation in integrated terrestrial system models at the larger catchment scale, *Frontiers in Water*, 5, <https://doi.org/10.3389/frwa.2023.1150999>, 2023.
- Li, M., Wu, P., Ma, Z., Lv, M., Yang, Q., and Duan, Y.: The decline in the groundwater table depth over the past four decades in China simulated by the Noah-MP land model, *Journal of Hydrology*, 607, 127 551, <https://doi.org/https://doi.org/10.1016/j.jhydrol.2022.127551>, 2022.
- 830 Lin, Y. S., Medlyn, B. E., Duursma, R. A., Prentice, I. C., Wang, H., Baig, S., Eamus, D., De Dios, V. R., Mitchell, P., Ellsworth, D. S., De Beeck, M. O., Wallin, G., Uddling, J., Tarvainen, L., Linderson, M. L., Cernusak, L. A., Nippert, J. B., Ocheltree, T. W., Tissue, D. T., Martin-StPaul, N. K., Rogers, A., Warren, J. M., De Angelis, P., Hikosaka, K., Han, Q., Onoda, Y., Gimeno, T. E., Barton, C. V., Bennie, J., Bonal, D., Bosc, A., Löw, M., Macinins-Ng, C., Rey, A., Rowland, L., Setterfield, S. A., Tausz-Posch, S., Zaragoza-Castells, J., Broadmeadow, M. S., Drake, J. E., Freeman, M., Ghannoum, O., Hutley, L. B., Kelly, J. W., Kikuzawa, K., Kolari, P., Koyama, K., Limousin, J. M., Meir, P., Da Costa, A. C., Mikkelsen, T. N., Salinas, N., Sun, W., and Wingate, L.: Optimal stomatal behaviour around the world, *Nature Climate Change*, 5, 459–464, <https://doi.org/10.1038/nclimate2550>, 2015.
- 835 Lindsay, J. B.: The Whitebox Geospatial Analysis Tools project and open-access GIS, *Proceedings of the GIS research UK 22nd annual conference*, 2014.

- Liu, J., Engel, B. A., Wang, Y., Wu, Y., Zhang, Z., and Zhang, M.: Runoff Response to Soil Moisture and Micro-topographic Structure on the Plot Scale, *Scientific Reports*, 9, 1–13, <https://doi.org/10.1038/s41598-019-39409-6>, 2019.
- 840 Lohila, A., Penttilä, T., Jortikka, S., Aalto, T., Anttila, P., Asmi, E., Aurela, M., Hatakka, J., Hellén, H., Henttonen, H., Hänninen, P., Kilkki, J., Kyllönen, K., Laurila, T., Lepistö, A., Lihavainen, H., Makkonen, U., Paatero, J., Rask, M., Sutinen, R., Tuovinen, J. P., Vuorenmaa, J., and Viisanen, Y.: Preface to the special issue on integrated research of atmosphere, ecosystems and environment at Pallas, *Boreal Environment Research*, 20, 431–454, 2015.
- 845 Lohila, A., Aalto, T., Aurela, M., Hatakka, J., Tuovinen, J. P., Kilkki, J., Penttilä, T., Vuorenmaa, J., Hänninen, P., Sutinen, R., Viisanen, Y., and Laurila, T.: Large contribution of boreal upland forest soils to a catchment-scale CH₄ balance in a wet year, *Geophysical Research Letters*, 43, 2946–2953, <https://doi.org/10.1002/2016GL067718>, 2016.
- Ma, L., He, C., Bian, H., and Sheng, L.: MIKE SHE modeling of ecohydrological processes: Merits, applications, and challenges, *Ecological Engineering*, 96, 137–149, <https://doi.org/10.1016/j.ecoleng.2016.01.008>, 2016.
- 850 Makhnykina, A. V., Prokushkin, A. S., Menyailo, O. V., Verkhovets, S. V., Tychkov, I. I., Urban, A. V., Rubtsov, A. V., Koshurnikova, N. N., and Vaganov, E. A.: The Impact of Climatic Factors on C₂ Emissions from Soils of Middle-Taiga Forests in Central Siberia: Emission as a Function of Soil Temperature and Moisture, *Russian Journal of Ecology*, 51, 46–56, <https://doi.org/10.1134/S1067413620010063>, 2020.
- Mäkisara, K., Katila, M., Peräsaari, J., and Tomppo, E.: The Multi-source National Forest Inventory of Finland – methods and results 2013. *Natural resources and bioeconomy studies 10/2016*, *Natural resources and bioeconomy studies*, p. 224, <http://urn.fi/URN:ISBN:978-952-326-186-0>, 2016.
- 855 Maneta, M. P. and Silverman, N. L.: A spatially distributed model to simulate water, energy, and vegetation dynamics using information from regional climate models, *Earth Interactions*, 17, <https://doi.org/10.1175/2012EI000472.1>, 2013.
- Manninen, T. and Jaaskelainen, E.: Pixel Based Multitemporal Sentinel-1 SAR Despeckling PIMSAR, *IEEE Geoscience and Remote Sensing Letters*, pp. 1–5, <https://doi.org/10.1109/lgrs.2021.3065300>, 2021.
- 860 Manninen, T., Jaaskelainen, E., Lohila, A., Korkiakoski, M., Rasanen, A., Virtanen, T., Muhic, F., Marttila, H., Ala-Aho, P., Markovaara-Koivisto, M., Liwata-Kenttala, P., Sutinen, R., and Hanninen, P.: Very High Spatial Resolution Soil Moisture Observation of Heterogeneous Subarctic Catchment Using Nonlocal Averaging and Multitemporal SAR Data, *IEEE Transactions on Geoscience and Remote Sensing*, pp. 1–17, <https://doi.org/10.1109/TGRS.2021.3109695>, 2021.
- Marttila, H., Lohila, A., Ala-Aho, P., Noor, K., Welker, J. M., Croghan, D., Mustonen, K., Meriö, L., Autio, A., Muhic, F., Bailey, H., Aurela, 865 M., Vuorenmaa, J., Penttilä, T., Hyöky, V., Klein, E., Kuzmin, A., Korpelainen, P., Kumpula, T., Rauhala, A., and Kløve, B.: Subarctic catchment water storage and carbon cycling – Leading the way for future studies using integrated datasets at Pallas, Finland, *Hydrological Processes*, 35, 1–19, <https://doi.org/10.1002/hyp.14350>, 2021.
- Mathijssen, P., Tuovinen, J.-P., Lohila, A., Aurela, M., Juutinen, S., Laurila, T., Niemelä, E., Tuittila, E.-S., and Välranta, M.: Development, carbon accumulation, and radiative forcing of a subarctic fen over the Holocene, *The Holocene*, 24, 1156–1166, 870 <https://doi.org/10.1177/0959683614538072>, 2014.
- Maxwell, R. M. and Condon, L. E.: Connections between groundwater flow and transpiration partitioning, *Science*, 353, 377–380, <https://doi.org/10.1126/science.aaf7891>, 2016.
- Maxwell, R. M., Chow, F. K., and Kollet, S. J.: The groundwater-land-surface-atmosphere connection: Soil moisture effects on the atmospheric boundary layer in fully-coupled simulations, *Advances in Water Resources*, 30, 2447–2466, 875 <https://doi.org/10.1016/j.advwatres.2007.05.018>, 2007.

- Mazzotti, G., Webster, C., Essery, R., and Jonas, T.: Increasing the Physical Representation of Forest-Snow Processes in Coarse-Resolution Models: Lessons Learned From Upscaling Hyper-Resolution Simulations, *Water Resources Research*, 57, 1–21, <https://doi.org/10.1029/2020WR029064>, 2021.
- 880 Menberu, M. W., Marttila, H., Ronkanen, A., Haghighi, A. T., and Kløve, B.: Hydraulic and Physical Properties of Managed and Intact Peatlands: Application of the Van Genuchten-Mualem Models to Peat Soils, *Water Resources Research*, 57, 1–22, <https://doi.org/10.1029/2020wr028624>, 2021.
- Meriö, L.-J., Rauhala, A., Ala-aho, P., Kuzmin, A., Korpelainen, P., Kumpula, T., Kløve, B., and Marttila, H.: Measuring the spatiotemporal variability of snow depth in subarctic environments using unmanned aircraft systems (UAS) – Part 2: Snow processes and snow-canopy interactions, *The Cryosphere Discussions*, 2023, 1–28, <https://doi.org/10.5194/tc-2022-242>, 2023.
- 885 Miguez-Macho, G., Fan, Y., Weaver, C. P., Walko, R., and Robock, A.: Incorporating water table dynamics in climate modeling: 2. Formulation, validation, and soil moisture simulation, *Journal of Geophysical Research Atmospheres*, 112, 1–16, <https://doi.org/10.1029/2006JD008112>, 2007.
- Moges, E., Demissie, Y., Larsen, L., and Yassin, F.: Review: Sources of Hydrological Model Uncertainties and Advances in Their Analysis, <https://doi.org/10.3390/w13010028>, 2021.
- 890 Moreno, J., Asensio, S., Berdugo, M., Gozalo, B., Ochoa, V., Pescador, D. S., Benito, B. M., and Maestre, F. T.: Fourteen years of continuous soil moisture records from plant and biocrust-dominated microsites, *Scientific Data*, 9, 1–7, <https://doi.org/10.1038/s41597-021-01111-6>, 2022.
- Muukkonen, P., Nevalainen, S., Lindgren, M., and Peltoniemi, M.: Spatial occurrence of drought-associated damages in Finnish boreal forests: Results from forest condition monitoring and GIS analysis, *Boreal Environment Research*, 20, 172–180, 2015.
- 895 Nakhavali, M., Lauerwald, R., Regnier, P., Guenet, B., Chadburn, S., and Friedlingstein, P.: Leaching of dissolved organic carbon from mineral soils plays a significant role in the terrestrial carbon balance, *Global Change Biology*, 27, 1083–1096, <https://doi.org/https://doi.org/10.1111/gcb.15460>, 2021.
- Niu, G. Y., Yang, Z. L., Mitchell, K. E., Chen, F., Ek, M. B., Barlage, M., Kumar, A., Manning, K., Niyogi, D., Rosero, E., Tewari, M., and Xia, Y.: The community Noah land surface model with multiparameterization options (Noah-MP): 1. Model description and evaluation with local-scale measurements, *Journal of Geophysical Research Atmospheres*, 116, 1–19, <https://doi.org/10.1029/2010JD015139>, 2011.
- 900 Niu, G. Y., Paniconi, C., Troch, P. A., Scott, R. L., Durcik, M., Zeng, X., Huxman, T., and Goodrich, D. C.: An integrated modelling framework of catchment-scale ecohydrological processes: 1. Model description and tests over an energy-limited watershed, *Ecohydrology*, 7, 427–439, <https://doi.org/10.1002/eco.1362>, 2014.
- Niu, Z., He, H., Peng, S., Ren, X., Zhang, L., Gu, F., Zhu, G., Peng, C., Li, P., Wang, J., Ge, R., Zeng, N., Zhu, X., Lv, Y., Chang, Q., Xu, Q., Zhang, M., and Liu, W.: A Process-Based Model Integrating Remote Sensing Data for Evaluating Ecosystem Services, *Journal of Advances in Modeling Earth Systems*, 13, e2020MS002451, <https://doi.org/https://doi.org/10.1029/2020MS002451>, 2021.
- 905 NLSF: National Land Survey of Finland Topographic Database, available at: <http://www.maanmittauslaitos.fi/en/e-services/open-data-file-download-service>, 2020.
- Noilhan, J. and Mahfouf, J. F.: The ISBA land surface parameterisation scheme, *Global and Planetary Change*, 13, 145–159, [https://doi.org/10.1016/0921-8181\(95\)00043-7](https://doi.org/10.1016/0921-8181(95)00043-7), 1996.
- 910 Nolan, M. and Fatland, D. R.: Penetration depth as a DInSAR observable and proxy for soil moisture, *IEEE Transactions on Geoscience and Remote Sensing*, 41, 532–537, <https://doi.org/10.1109/TGRS.2003.809931>, 2003.

- Nousu, J.-P., Lafaysse, M., Mazzotti, G., Ala-aho, P., Marttila, H., Cluzet, B., Aurela, M., Lohila, A., Kolari, P., Boone, A., Fructus, M., and Launiainen, S.: Modelling snowpack dynamics and surface energy budget in boreal and subarctic peatlands and forests, *EGU*sphere, 2023, 1–52, <https://doi.org/10.5194/egusphere-2023-338>, 2023.
- 915 Nousu, J.-P., Leppä, K., and Launiainen, S.: LukeEcomod/SpaFHy_v1_Pallas_2D, <https://doi.org/10.5281/zenodo.10820456>, 2024a.
- Nousu, J.-P., Leppä, K., Marttila, H., Ala-Aho, P., Mazzotti, G., Manninen, T., Korkiakoski, M., Aurela, M., Lohila, A., and Launiainen, S.: Multi-scale soil moisture data and process-based modeling reveal the importance of lateral groundwater flow in a subarctic catchment, <https://doi.org/10.5281/zenodo.10820563>, 2024b.
- 920 O’Callaghan, J. F. and Mark, D. M.: The extraction of drainage networks from digital elevation data, *Computer Vision, Graphics, and Image Processing*, 28, 323–344, [https://doi.org/10.1016/S0734-189X\(84\)80011-0](https://doi.org/10.1016/S0734-189X(84)80011-0), 1984.
- Olson, D. M., Dinerstein, E., Wikramanayake, E. D., Burgess, N. D., Powell, G. V., Underwood, E. C., D’Amico, J. A., Itoua, I., Strand, H. E., Morrison, J. C., Loucks, C. J., Allnutt, T. F., Ricketts, T. H., Kura, Y., Lamoreux, J. F., Wettengel, W. W., Hedao, P., and Kassem, K. R.: Terrestrial ecoregions of the world: A new map of life on Earth, *BioScience*, 51, 933–938, [https://doi.org/10.1641/0006-3568\(2001\)051\[0933:TEOTWA\]2.0.CO;2](https://doi.org/10.1641/0006-3568(2001)051[0933:TEOTWA]2.0.CO;2), 2001.
- 925 Panday, S. and Huyakorn, P. S.: A fully coupled physically-based spatially-distributed model for evaluating surface/subsurface flow, *Advances in Water Resources*, 27, 361–382, <https://doi.org/10.1016/j.advwatres.2004.02.016>, 2004.
- Pomeroy, J. W., Parviainen, J., Hedstrom, N., and Gray, D. M.: Coupled modelling of forest snow interception and sublimation, *Hydrological Processes*, 12, 2317–2337, [https://doi.org/10.1002/\(SICI\)1099-1085\(199812\)12:15<2317::AID-HYP799>3.0.CO;2-X](https://doi.org/10.1002/(SICI)1099-1085(199812)12:15<2317::AID-HYP799>3.0.CO;2-X), 1998.
- 930 Quast, R., Wagner, W., Bauer-Marschallinger, B., and Vreugdenhil, M.: Soil moisture retrieval from Sentinel-1 using a first-order radiative transfer model—A case-study over the Po-Valley, *Remote Sensing of Environment*, 295, 113651, <https://doi.org/https://doi.org/10.1016/j.rse.2023.113651>, 2023.
- Räsänen, J.: Snow conditions in northern Europe: The dynamics of interannual variability versus projected long-term change, *Cryosphere*, 15, 1677–1696, <https://doi.org/10.5194/tc-15-1677-2021>, 2021.
- 935 Raleigh, M. S., Lundquist, J. D., and Clark, M. P.: Exploring the impact of forcing error characteristics on physically based snow simulations within a global sensitivity analysis framework, *Hydrology and Earth System Sciences*, 19, 3153–3179, <https://doi.org/10.5194/hess-19-3153-2015>, 2015.
- Räsänen, A., Manninen, T., Korkiakoski, M., Lohila, A., and Virtanen, T.: Predicting catchment-scale methane fluxes with multi-source remote sensing, *Landscape Ecology*, 36, 1177–1195, <https://doi.org/10.1007/s10980-021-01194-x>, 2021.
- 940 Räsänen, A., Tolvanen, A., and Kareksela, S.: Monitoring peatland water table depth with optical and radar satellite imagery, *International Journal of Applied Earth Observation and Geoinformation*, 112, 102866, <https://doi.org/https://doi.org/10.1016/j.jag.2022.102866>, 2022.
- Robinson, D., Campbell, C., Hopmans, J., Hornbuckle, B., Jones, S., Knight, R., Ogden, F., Selker, J., and Wendroth, O.: Soil Moisture Measurement for Ecological and Hydrological Watershed-Scale Observatories: A Review All rights reserved. No part of this periodical may be reproduced or transmitted in any form or by any means, electronic or mechanical, including photocopyin, *Vadose Zone J.*, 7, 358–389, 2008.
- 945 Ruosteenoja, K., Markkanen, T., Venäläinen, A., Räsänen, P., and Peltola, H.: Seasonal soil moisture and drought occurrence in Europe in CMIP5 projections for the 21st century, *Climate Dynamics*, 50, 1177–1192, <https://doi.org/10.1007/s00382-017-3671-4>, 2018.
- Salmivaara, A., Launiainen, S., Perttunen, J., Nevalainen, P., Pohjankukka, J., Ala-Ilomäki, J., Sirén, M., Laurén, A., Tuominen, S., Uusitalo, J., Pahikkala, T., Heikkonen, J., and Finér, L.: Towards dynamic forest trafficability prediction using open spatial data, hydrological modelling and sensor technology, *Forestry*, 93, 662–674, <https://doi.org/10.1093/FORESTRY/CPAA010>, 2021.
- 950

- Schneider, J., Jungkunst, H. F., Wolf, U., Schreiber, P., Gazovic, M., Miglovets, M., Mikhaylov, O., Grunwald, D., Erasmi, S., Wilmking, M., and Kutzbach, L.: Russian boreal peatlands dominate the natural European methane budget, *Environmental Research Letters*, 11, <https://doi.org/10.1088/1748-9326/11/1/014004>, 2016.
- Seibert, J. and Vis, M. J. P.: Teaching hydrological modeling with a user-friendly catchment-runoff-model software package, *Hydrology and Earth System Sciences*, 16, 3315–3325, <https://doi.org/10.5194/hess-16-3315-2012>, 2012.
- 955 Seneviratne, S. I., Corti, T., Davin, E. L., Hirschi, M., Jaeger, E. B., Lehner, I., Orlowsky, B., and Teuling, A. J.: Investigating soil moisture-climate interactions in a changing climate: A review, *Earth-Science Reviews*, 99, 125–161, <https://doi.org/10.1016/j.earscirev.2010.02.004>, 2010.
- Shellito, P. J., Kumar, S. V., Santanello, J. A., Lawston-Parker, P., Bolten, J. D., Cosh, M. H., Bosch, D. D., Collins, C. D. H., Livingston, S., Prueger, J., Seyfried, M., and Starks, P. J.: Assessing the Impact of Soil Layer Depth Specification on the Observability of Modeled Soil Moisture and Brightness Temperature, *Journal of Hydrometeorology*, 21, 2041 – 2060, <https://doi.org/10.1175/JHM-D-19-0280.1>, 2020.
- 960 Sidle, R. C.: Strategies for smarter catchment hydrology models: incorporating scaling and better process representation, *Geoscience Letters*, 8, <https://doi.org/10.1186/s40562-021-00193-9>, 2021.
- Singh, N. K., Emanuel, R. E., McGlynn, B. L., and Miniati, C. F.: Soil Moisture Responses to Rainfall: Implications for Runoff Generation, *Water Resources Research*, 57, e2020WR028 827, <https://doi.org/https://doi.org/10.1029/2020WR028827>, 2021.
- 965 Skaggs, R. W.: A Water Management Model for Artificially Drained Soils, North Carolina Agri. Exp. Station Tech. Bul, North Carolina Agricultural Research Service, <https://books.google.fi/books?id=F3JRAQAAMAAJ>, 1980.
- Skofronick-Jackson, G., Petersen, W. A., Berg, W., Kidd, C., Stocker, E. F., Kirschbaum, D. B., Kakar, R., Braun, S. A., Huffman, G. J., Iguchi, T., Kirstetter, P. E., Kummerow, C., Meneghini, R., Oki, R., Olson, W. S., Takayabu, Y. N., Furukawa, K., and Wilhelm, T.: The Global Precipitation Measurement (GPM) Mission for Science and Society, *Bulletin of the American Meteorological Society*, 98, 1679 – 1695, <https://doi.org/10.1175/BAMS-D-15-00306.1>, 2017.
- 970 Smith, B., Prentice, I. C., and Sykes, M. T.: Representation of vegetation dynamics in the modelling of terrestrial ecosystems: comparing two contrasting approaches within European climate space, *Global Ecology and Biogeography*, 10, 621–637, <https://doi.org/https://doi.org/10.1046/j.1466-822X.2001.t01-1-00256.x>, 2001.
- Stenberg, L., Leppä, K., Launiainen, S., Laurén, A., Hökkä, H., Sarkkola, S., Saarinen, M., and Nieminen, M.: Measuring and Modeling the Effect of Strip Cutting on the Water Table in Boreal Drained Peatland Pine Forests, *Forests*, 13, <https://doi.org/10.3390/f13071134>, 2022.
- Stuefer, S. L., Kane, D. L., and Dean, K. M.: Snow Water Equivalent Measurements in Remote Arctic Alaska Watersheds, *Water Resources Research*, 56, 1–12, <https://doi.org/10.1029/2019WR025621>, 2020.
- 975 Tang, J., Pilesjö, P., Miller, P. A., Persson, A., Yang, Z., Hanna, E., and Callaghan, T. V.: Incorporating topographic indices into dynamic ecosystem modelling using LPJ-GUESS, *Ecohydrology*, 7, 1147–1162, <https://doi.org/https://doi.org/10.1002/eco.1446>, 2014.
- Thornton, J. M., Therrien, R., Mariéthoz, G., Linde, N., and Brunner, P.: Simulating Fully-Integrated Hydrological Dynamics in Complex Alpine Headwaters: Potential and Challenges, *Water Resources Research*, 58, <https://doi.org/10.1029/2020WR029390>, 2022.
- Toca, L., Artz, R. R. E., Smart, C., Quaife, T., Morrison, K., Gimona, A., Hughes, R., Hancock, M. H., and Klein, D.: Potential for Peatland Water Table Depth Monitoring Using Sentinel-1 SAR Backscatter: Case Study of Forsinard Flows, Scotland, UK, <https://doi.org/10.3390/rs15071900>, 2023.
- 985 Tyystjärvi, V., Kempainen, J., Luoto, M., Aalto, T., Markkanen, T., Launiainen, S., Kieloaho, A. J., and Aalto, J.: Modelling spatio-temporal soil moisture dynamics in mountain tundra, *Hydrological Processes*, 36, <https://doi.org/10.1002/hyp.14450>, 2022.

- van Genuchten, M. T.: A Closed-form Equation for Predicting the Hydraulic Conductivity of Unsaturated Soils, *Soil Science Society of America Journal*, 44, 892–898, <https://doi.org/10.2136/sssaj1980.03615995004400050002x>, 1980.
- 990 Venäläinen, A., Lehtonen, I., Laapas, M., Ruosteenoja, K., Tikkanen, O.-P., Viiri, H., Ikonen, V.-P., and Peltola, H.: Climate change induces multiple risks to boreal forests and forestry in Finland: A literature review, *Global Change Biology*, 26, 4178–4196, <https://doi.org/https://doi.org/10.1111/gcb.15183>, 2020.
- Wang, T., Zhang, H., Zhao, J., Wu, R., Li, H., Guo, X., and Zhao, H.: Increased atmospheric moisture demand induced a reduction in the water content of boreal forest during the past three decades, *Agricultural and Forest Meteorology*, 342, 109 759, 995 <https://doi.org/10.1016/j.agrformet.2023.109759>, 2023.
- Webster, C., Essery, R., Mazzotti, G., and Jonas, T.: Using just a canopy height model to obtain lidar-level accuracy in 3D forest canopy shortwave transmissivity estimates, *Agricultural and Forest Meteorology*, 338, 109 429, <https://doi.org/10.1016/j.agrformet.2023.109429>, 2023.
- Williams, T. G. and Flanagan, L. B.: Effect of changes in water content on photosynthesis, transpiration and discrimination against ^{13}C and $\text{C}_{18}\text{O}_{16}\text{O}$ in *Pleurozium* and *Sphagnum*, *Oecologia*, 108, 38–46, <https://doi.org/10.1007/BF00333212>, 1996.
- 1000 Wood, E. F., Roundy, J. K., Troy, T. J., van Beek, L. P. H., Bierkens, M. F. P., Blyth, E., de Roo, A., Döll, P., Ek, M., Famiglietti, J., Gochis, D., van de Giesen, N., Houser, P., Jaffé, P. R., Kollet, S., Lehner, B., Lettenmaier, D. P., Peters-Lidard, C., Sivapalan, M., Sheffield, J., Wade, A., and Whitehead, P.: Hyperresolution global land surface modeling: Meeting a grand challenge for monitoring Earth’s terrestrial water, *Water Resources Research*, 47, <https://doi.org/https://doi.org/10.1029/2010WR010090>, 2011.
- 1005 Yu, L., Gao, W., Shamshiri, R. R., Tao, S., Ren, Y., Zhang, Y., and Su, G.: Review of research progress on soil moisture sensor technology, *International Journal of Agricultural and Biological Engineering*, 14, 32–42, <https://doi.org/10.25165/j.ijabe.20211404.6404>, 2021.
- Yu, S., Lu, F., Zhou, Y., Wang, X., Wang, K., Song, X., and Zhang, M.: Evaluation of Three High-Resolution Remote Sensing Precipitation Products on the Tibetan Plateau, <https://doi.org/10.3390/w14142169>, 2022.
- Zeng, Y., Xie, Z., Liu, S., Xie, J., Jia, B., Qin, P., and Gao, J.: Global Land Surface Modeling Including Lateral Groundwater Flow, *Journal of Advances in Modeling Earth Systems*, 10, 1882–1900, <https://doi.org/https://doi.org/10.1029/2018MS001304>, 2018.
- 1010 Zhang, F. and Zhou, G.: Estimation of Canopy Water Content by Means of Hyperspectral Indices Based on Drought Stress Gradient Experiments of Maize in the North Plain China, <https://doi.org/10.3390/rs71115203>, 2015.
- Zhang, H., Liu, J., Li, H., Meng, X., and Ablikim, A.: The Impacts of Soil Moisture Initialization on the Forecasts of Weather Research and Forecasting Model: A Case Study in Xinjiang, China, <https://doi.org/10.3390/w12071892>, 2020a.
- 1015 Zhang, H., Tuittila, E. S., Korrensalo, A., Räsänen, A., Virtanen, T., Aurela, M., Penttilä, T., Laurila, T., Gerin, S., Lindholm, V., and Lohila, A.: Water flow controls the spatial variability of methane emissions in a northern valley fen ecosystem, *Biogeosciences*, 17, 6247–6270, <https://doi.org/10.5194/bg-17-6247-2020>, 2020b.
- Zhang, Y., Gong, J., Sun, K., Yin, J., and Chen, X.: Estimation of soil moisture index using multi-temporal Sentinel-1 images over Poyang Lake ungauged zone, *Remote Sensing*, 10, 1–19, <https://doi.org/10.3390/rs10010012>, 2018.